8-2010

State Estimation for diffusion systems using a Karhunen-Loeve-Galerkin Reduced-Order Model

Justin Mattimore
Clemson University, jmattim@clemson.edu

State Estimation for diffusion systems using a Karhunen-Loéve-Galerkin Reduced-Order Model

---

A Dissertation
Presented to
the Graduate School of
Clemson University

In Partial Fulfillment
of the Requirements for the Degree
Master of Science
Electrical Engineering

---

by
Justin P. Mattimore
August 2010

Accepted by:
Dr. Richard E. Groff, Committee Chair
Dr. Timothy Burg
Dr. Adam Hoover

Abstract

This thesis focuses on generating a continuous estimate of state using a small number of sensors for a process modeled by the diffusion partial differential equation(PDE). In biological systems the diffusion of oxygen in tissue is well described by the diffusion equation, also known by biologists as Fick's first law. Mass transport of many other materials in biological systems are modeled by the diffusion PDE such as CO_2, cell signaling factors, glucose and other biomolecules.

Estimating the state of a PDE is more formidable than that of a system described by ordinary differential equations (ODEs). While the state variables of the ODE system are finite in number, the state variables of the PDE are distributed in the spatial domain and infinite in number. Reduction of the number of state variables to a finite small number which is tractable for estimation will be accomplished through use of the Karhunen-Loéve-Galerkin method for model order reduction. The model order reduction is broken into two steps, (i) determine an appropriate set of basis functions and (ii) project the PDE onto the set of candidate basis functions. The Karhunen-Loéve expansion is used to decompose a set of observations of the system into the principle modes composing the system dynamics. The observations may be obtained through numerical simulation or physical experiments that encompass all dynamics that the reduced-order model will be expected to reproduce. The PDE is then projected onto a small number of basis functions using the linear Galerkin method, giving a small set of ODEs which describe the system dynamics. The reduced-order model obtained from the Karhunen-Loéve-Galerkin procedure is then used with a Kalman filter to estimate the system state.

Performance of the state estimator will be investigated using several numerical experiments. Fidelity of the reduced-order model for several different numbers of basis functions will be compared against a numerical solution considered to be the true solution of the continuous problem. The efficiency of the empirical basis compared to an analytical basis will be examined. The reduced-

order model will then be used in a Kalman filter to estimate state for a noiseless system and then a noisy system. Effects of sensor placement and quantity are evaluated.

A test platform was developed to study the estimation process to track state variables in a simple non-biological system. The platform allows the diffusion of dye through gelatin to be monitored with a camera. An estimate of dye concentration throughout the entire volume of gelatin will be accomplished using a small number of point sensors, i.e. pixels selected from the camera. The estimate is evaluated against the actual diffusion as captured by the camera. This test platform will provide a means to empirically study the dynamics of diffusion-reaction systems and associated state estimators.

Acknowledgments

I would like to thank my advisors Dr. Richard E. Groff and Dr. Timothy Burg for many enlightening discussions and patient explanations greatly contributing to my knowledge. Without their confidence in me and support this thesis would not have been possible. I would also like to thank Dr. Timothy Burg and Dr. Karen Burg for supporting my studies through a research assistantship sponsored by the National Science Foundation.

Table of Contents

List of Tables

List of Figures

Chapter 1

Introduction

The transport process of mass diffusing in a medium describes many physical processes. The diffusion or heat equation is written as

$$\frac{\partial u(x,t)}{\partial t} = D\frac{\partial^2 u(x,t)}{\partial x^2} \quad x \in \Omega \quad t > 0 \tag{1.1}$$

where u describes the mass concentration, D is a dimensionless real valued constant determining the rate of diffusion on the domain Ω. The second order derivative, the Laplacian, is smooth. Many biological and chemical processes are more accurately described by the advection-reaction-diffusion equation described by the partial differential equation (PDE) of the form

$$\frac{\partial u(x,t)}{\partial t} = a\frac{\partial u(x,t)}{\partial x} + D\frac{\partial^2 u(x,t)}{\partial x^2} + F(u(x,t)) \quad x \in \Omega \quad t > 0 \tag{1.2}$$

Where $F(u)$ is a function describing the reaction process and the term $a\frac{\partial u}{\partial x}$ is the advection or flow term. The advection term is not smooth and allows discontinuities to be propagated in the solution, creating difficulty in solving the advection-reaction-diffusion equation. Restricting study to pure diffusion will simplify analysis while allowing application of the major components of this thesis to more complex systems governed by PDEs such as the advection-reaction-diffusion equation.

Making practical use of systems governed by PDEs requires the ability to estimate the state of the system and/or to control it. The former requisite of estimating state is the primary concern of this thesis. Observing the state of a PDE is a more formidable task than most systems

described by ordinary differential equations (ODE). For an ODE system, a finite number of states are described by the ODEs. The states may be observed using a finite number of measurement sensors in accordance with the intrinsic system requirements for observing the system. Systems described by partial differential equations do not have a finite number of states. Techniques will be presented for reducing the infinite number of state variables into a small subset of state variables and estimating the system state with a finite set of measurement sensors.

This thesis focuses on generating a (near) continuous estimate of state for a process well modeled by the diffusion partial differential equation using a small number of sensors. In biological systems the diffusion of oxygen in tissue is well described by the diffusion equation, also known by biologists as Fick's first law. A test platform will be developed to show the application of the estimation process to track state variables in a simple non-biological system with clear application to biological systems. The mass transport process of oxygen diffusion in tissue and hydrogels such as collagen is similar to the diffusion of dye in gelatin. An estimate of dye concentration throughout the entire volume of gelatin will be accomplished using a small number of sensors. The methods for generating the state estimate require *a priori* knowledge of the system's structure and parameters. This amounts to limiting gelatin to a known geometry and size (structure) and the same gelatin stiffness and dye molecule (parameters). From an application standpoint this implies the ability to know the system structure of a biological system such as an engineered tissue. Future application of work extended from this thesis is state estimation of biological system using a mathematical tumor model. The utility of developing a state estimator for use in a living *in vitro* tumor model is contingent on ability to characterize the system with a mathematical model and sense the state at discrete points. Constructing a tumor tissue with a known and controlled structure implies the ability to engineer and build tissue. The realizability of these points will be shown through a literature survey. First, the ability to model biological processes, especially cancer, using mathematical models is shown. Next biological systems in the context of control systems is motivated on a subcellular level (gene expression) with application oriented to control of tumor growth using mathematical models. Biological sensing for feedback and control using optical contactless non-invasive point sensors are shown to be in development.

1.1 Mathematical Biological (*in silico*) Models

Mathematical *in silico* models have been employed to model a multitude of physiological phenomena including cellular signaling pathways [127] [2] [129], molecular events [111] [32], vascular fluid dynamics [109] [21], tumor cell migration [4] [5] , and solid tumor growth. It should be noted that use of the phrase "biological model" should connote the description of phenomena in terms of a mathematical model; biologists define a biological model as a way of doing things which bring about a known result, rather than as a mathematical model [71]. The principle interest will be restricted to mathematical models of tumor growth and pharmacodynamics (response of drug-cell interaction).

Description of physiological process in rigorous mathematical form has a short history [7]. An example of early deterministic descriptions of physiological processes is Hill's research of diffusion of oxygen and lactic acid in and out of tissues. Hill recognized the importance of diffusion in many key physiological processes [56]. Thomlinson and Gray used the idea of oxygen diffusion in tissue to develop a model relating consumption and diffusion of oxygen in avascular tumors. The researchers were able to develop a model which predicting tumor cell necrosis relative to tumor size in close agreement with empirical observations of 160 tumor masses [123]. Laird [73] and later Burton [22] devised diffusion growth models fitting rate of growth to a Gompertzian (sigmoidal) curve.

Study of avascular tumors continued including surface tension causing living tumors cells to maintain a compact mass, diffusion of necrotic cell remains outward [50], growth inhibitors [98], and extension to two and three dimensions [118]. Greene first noticed growth of tumors implanted in the guinea pig eye were limited by vasoproliferation [49]. Folkman noted inability of tumors to grow beyond a certain size threshold without forming new vasculature [41]. The compound responsible for angiogenesis was isolated [42] and angiogensis as a necessary mechanism for tumor proliferation was proposed in Folkman's seminal work [40]. Realization of the link between ability of tumors to grow vasculature (angiogenesis) through experimental work made requisite the modeling of angiogenic tumor models. Despite this, work has continued in the area of avascular tumor models, including inclusion of spatially depending diffusion coefficient, autocrine (self) and paracrine (neighboring) signaling, apoptosis (programmed cell death) and proliferation [7].

The development of avascular tumor models relying on the diffusion process makes apparent the importance of the diffusion equation in tumor modeling but also elucidates the major deficiency of avascular tumor models - the models lack ability to predict metastasis, tumor cell invasion,

angiogenesis, etc. In depth coverage of tumor model development may be found in [7] and [82] [26].

This abbreviated review of tumor growth models merely discusses avascular tumor growth which only accounts for tumor size, metabolite diffusion and at most some growth factors and only on one length scale. Complex tumor models describe phenomena on multiple length scales, at the tissue and cellular level. Multiscale models have already been established in chemical processes [84]. Describing cellular response to signaling factors and adaptation stress is important to developing models able to predict angiogenesis and resistance to treatment [23] [4] [5] [108].

Diffusion gradients of anticancer drugs in avascular tumors have been shown to hinder drug delivery in animal experiments [105] and in clinical application [75]. Evidence shows an increase in drug resistance of tumor cells is affected by the diffusion gradient as well as the cell type [119]. Frieboes, et. al. investigated tumor response to a cytotoxic drug comparing experimental and *in silico* predictions. Tumor response to concentration of nutrients, oxygen and anticancer drug were included in a multiscale model. Parameters for the 3D mathematical model are recovered by extrapolating values found from cell monolayers. MCF-7 wild type (chemosensitive) and MCF-740F (chemo-resistant) were cultured into multicellular spheroids. Cell viability for the chemosensitive and chemo-resistant cells types are found for several concentrations of the anticancer drug Doxorubicin using the mathematical model and experiment with cells. The math model produced results similar to the observations made in the experiment [43].

1.2 Biological Systems in a Control Context

Mathematical modeling of biological systems with deterministic differential equations casts the biological system into a palpable form for control. This thesis is concerned with state estimation; future work building on this thesis will include control. Therefore, it is worthwhile to confirm that models fit for controller synthesis. Cellular response is discussed in the context of control, motivating use of *in silico* models for synthesis of controllers.

The physical process of diffusion, describing mass transport such as metabolites, katabolites and signaling factors through media, is well established. Using the knowledge of fundamental processes such as diffusion does not give an obvious answer to what response the cells will have in response to those chemicals. It has been demonstrated that cellular responses do obey deterministic models for phenomena such as division, death, signaling and motility. Casting the cellular system in

a control theoretic framework is natural and allows description of phenomena in terms of feedback loops [120]. Novak and Tyson describe a simple example to demonstrate the biological control loop. The authors consider a protein which governs the transcription of a protein's corresponding gene. The production of the protein is regulated by decay of the protein and production based on concentration. Intermediate reactions and transcription time introduce a delay in synthesis. The delay causes continual up-regulation of synthesis until the protein appears in the cell. The overshoot due to delay results in limit cycle oscillations of the protein concentration in the cell [95]. The process is modeled by Michaelis-Menten kinetics, an ordinary differential equation. Synthesis of the protein may be viewed as a negative feedback system [120] [127] [95].

Ledzewicz and Schättler developed an optimal bang-bang controller for a two compartment cancer model. The two compartment division of the model splits the tumor dynamics into a growth phase and into a growth plus mitosis phase which is the only time the cancer drug is available [76]. Hahndeldt developed a 2D mathematical angiogenesis model which is biologically verified [54]. The Hahndeldt model approximates a PDE system describing angiogenesis with an ODE system. Ledzewicz and Schättler developed optimal control laws using an optimal singular arc to reduce tumor volume using the Hahnfeldt angiogenic model [77]. Nath developed an adaptive control law for the angiogenic Hahnfeldt model driving the tumor to a minimized volume [90]. Fister and Panetta develop an optimal controller for an ODE model characterizing bone marrow cancer. A control law for cycle-specific anticancer drug delivery based on Pontryagin's maximum principle extremizing a cost functional maximizing bone mass and dose simultaneously [38]. Kirschner synthesizes an optimum controller for an ODE system describing HIV. A controller based on Pontryagin's maximum principle is formuated to extremize a functional weighting T cell count and drug concentration [69]. Groups Castiglione & Piccoli and Pillis & Radunskaya each propose optimal controls for ODE systems describing immune response in presecence of cancer. Pontryagin's maximum principle is used to synthesize controllers boosting immune response [25] [30].

Nearly all control models for biological systems found in a literature search are synthesized for ODE systems which approximate a tumor model with special restrictions. Controlling response for more complex systems require use of the PDE governing the system. The difficulty in synthesizing PDE controllers or estimators has been addressed by chemical engineering and electrical engineering communities.

1.3 Sensing in Biological Systems

The opening remarks indicate the state for a model with a known physical structure will be estimated. Knowledge of the system structure will be necessary for generating a state estimate using a small number of sensors. Excising tissue samples from animals for biological experiments does not provide a repeatable test sample. Variations in tissue composition arise from many factors making tissue properties, for example the diffusion coefficient may vary from sample to sample. Generating a tissue sample allows control of tissue composition and known placement of measurement sensors. Techniques for generating large scale tissue samples have been proposed by many researchers. Most techniques may be classified as a scaffolding and cell seeding [91] or free-form fabrication using micro pipettes [66] or inkjet cartridges for deposition [89] [103]. Cell seeding relies on self-assembly [91] and does not have direct control over composition of cell populations. The free-form fabrication techniques allow deposition several cell types and better control of cell placement. Placing biosensors in samples of known composition will permit state estimation using a small number of sensors.

New sensor technologies for sensing in biological systems are being developed allowing for non-invasive optical contactless sensing in the form of films and points sensors ranging from micron to nano scale [88]. Sensors for imaging biomolecules, CO_2, oxygen and pH are being developed [20]. Oxygen sensor development has been driven in part by the tissue engineering community. Construction of *ex vivo* tissue replacements of bone and cartilage of appreciable size have not been possible [65]. Evidence indicating delivery of nutrients and oxygen are insufficient [34]. Sensing and oxygen delivery are recognized challenges in constructing engineered tissue [65].

Metal chelates form the basis for contactless optical biosensing. Lanthanide chelates such as Europium(III) chelates provide a narrow excitation window suitable for sensing [55]. Many Europium(III) chelates suffer from strong temperature-dependent luminescence and are excitable in the UV range which may cause background fluorescence. Some visible Europium(III) chelates have been developed which may be excited by normal LED light sources [19]. Transition metal complexes such as palladium(II), platinum(II) and ruthenium(II) have characteristic phosphorescence times and are applicable to a wide gamut of biological sensing [99] [70].

Papkovsky, et. al propose a class of porphyrin ketones using palladium(II) and platinum(II) for use with oxygen sensing. Advantages of the new porphyrin ketone complexes are better chemical stability and better photo response [100]. Borisov, et. al propose poly beads as a material for

manufacture of optical nanosensors. The authors prepare sensors each capable of measuring either oxygen, temperature, pH, copper or chloride. Performance of the 245nm beads are characterized for several different dyes. Leaching, storage stability and toxicity are also investigated [20]. McNamara and Rosenzweig encapsulate ruthenium cloride ($Ru(phen)_3$) in liposomes producing sub-micron sensors [86]. Im, et. al develop dual lumiphor oxygen sensors polystyrene beads loaded with octa-ethyl-porphyrin (SiOEP) and platinum octa-ethyl-porphyrin (PtOEP). The dual lumiphor schema provides a self reference for calibration [60].

Kellner, et. al measured the oxygen gradient in native bovine articular cartilage and engineered cartilage. Engineered cartilage constructs were constructed by digesting the bovine articular cartilage with type II collagenase and seeding PGA scaffolds. Samples were affixed to a platinum(II)-octaethyl-porphyrin film using alginate crosslinked with $CaCl_2$. The 5×2mm discs were photographed and oxygen partial pressures were calculated on a pixel by pixel basis using the hue of the calibrated sensors yielding the oxygen gradient in 2D [65].

Chapter 2

Background

Estimation and control of dynamic systems require a system model and the ability to sense the state of a system. For traditional controls techniques, a system uses a finite number of sensors and a finite number of actuators to control a finite number of system states. In many applications, the system model may have many or an infinite number of states yet still have a finite number of sensors and actuators. For example, the diffusion of oxygen in a medium is described by the diffusion equation

$$\frac{\partial u}{\partial t} = D\frac{\partial^2 u}{\partial x^2} \quad x \in \Omega \quad t > 0 \tag{2.1}$$

where u is the mass concentration, x is position, t is time, and D is a constant known as the diffusion coefficient The diffusion equation cannot be analyzed using classical controls techniques as the system is truly distributed having an infinite number of state variables. Systems with many or infinite number of state variables are said to be high dimensional systems or infinite dimensional systems.

The goal of this thesis is to estimate the state of a diffusion process, a high dimensional system, using a small and computationally tractable mathematical model. This goal will be met by limiting the admissible PDEs to systems described by the diffusion equation. A desirable property of the diffusion equation will be exploited; the dominant slow dynamic behavior of the system may be described by a finite set of system modes while discarding the infinite dimensional complement. A model which approximates a high dimensional system with a small number of states will be

presented. First, analytical and numerical solution techniques for solving the diffusion equation along with properties of the diffusion equation are presented. Secondly, a method for reducing the state dimension of the diffusion equation using a set of empirical basis functions and a the linear Galerkin projection. Lastly, the Kalman state estimator is introduced. Using the aforementioned three components a state estimator is constructed.

2.1 Reduced Order Model Motivation

The solution to the diffusion PDE will be covered using several techniques. The high dimensionality becomes obvious when the numerical solutions are implemented. For the (spatial) one-dimensional case of the diffusion PDE a discretization of a spatial domain from 0 to 1 into 100 increments may be solved using numerical solvers faster than real time, depending on the solver. The physical process of diffusion is most accurately described in two and three spatial dimensions. Simulating the diffusion PDE in two and three dimensions using a spatial discretization similar to the 1D case in each direction makes the computational burden very apparent. Decreasing the number of points in the discretization will allow for faster computation time at the expense of solution accuracy. The order of the model refers to the number of discretization points in the solution. For the 1D case described the dimension is 100 while the 2D case is 10,000 and the 3D case is an incomprehensible 1,000,000. Reducing the order of the model while retaining an accurate description of the dynamics is desired. A method will be presented which produces high fidelity solutions using reduced order models yet retaining a fine spatial discretization.Particularly the dynamical system will be expressed as a system of ODEs

$$\frac{d\tilde{x}}{dt} = A\tilde{x} + \eta_s$$

$$\tilde{y} = C\tilde{x} + \varepsilon$$

2.2 Diffusion Partial Differential Equation (PDE)

The diffusion process is described by

$$\frac{\partial u}{\partial t} = D\frac{\partial^2 u}{\partial x^2} \quad x \in \Omega \quad t > 0 \tag{2.2}$$

The diffusion equation is said to be a parabolic PDE; eventually the parabolic nature of the diffusion PDE will be exploited allowing separation of the system into dominant dynamic behavior and an infinite dimensional complement which will be discarded. The dominant behavior is retained forming a reduced order model. The performance of the reduced order model will be compared with known true solutions to the diffusion equation. Tools prsesented to obtains solutions through several methods will be presented. The classical spectral solution method using a Fourier cosine basis is developed. Methods for numerically approximating the diffusion equation are presented in two forms - an explicit Euler solution and a semi-analytical method for solving PDEs through discretization into a set of ordinary differential equations (ODE). The machinery used in forming the explicit Euler solution is exploited for finding the discrete Laplacian, similar to the diffusion operator, for use in finding the reduced order model.

2.2.1 Properties of the Diffusion PDE

The diffusion (or heat) equation is a parabolic partial differential equation. In one dimension it is given explicitly as

$$\frac{\partial u}{\partial t} = \alpha \frac{\partial^2 u}{\partial x^2} \quad x \in (x_0, x_\ell) \quad t > 0 \tag{2.3}$$

or alternatively

$$\frac{\partial u}{\partial t} = D\Delta u = D\nabla^2 u \tag{2.4}$$

Where α is the diffusion coefficient. The right hand side of 2.4 is an alternative expression with the coefficient D a real valued constant. The second order derivative in space is also referred to as the Laplacian.

Writing the PDE in subscript notation will be more succinct for the finite difference expressions

$$u_t = \alpha u_{xx} \tag{2.5}$$

In two dimensions the diffusion equation is written

$$\frac{\partial u}{\partial t} = \alpha \frac{\partial^2 u}{\partial x^2} + \alpha \frac{\partial^2 u}{\partial y^2} \quad x \in (x_0, x_\ell) \quad t > 0 \tag{2.6}$$

or equivalently

$$u_t = \alpha u_{xx} + \alpha u_{yy} \tag{2.7}$$

The problems studied will be initial boundary value problems. The state is known at initial time and the boundary of the spatial domain must satisfy the boundary conditions for all time. The boundary conditions determine if the system solution will dissipate, grow or be conserved. The boundary conditions in a 1D domain are defined as

Dirichlet	Neumann	Robin	
$u(x_0,t) = a$	$\frac{du(x_0,t)}{dx} = a$	$u(x_0,t) + \frac{du(x_0,t)}{dx} = a$	$t \in [0, t_f]$
$u(x_\ell,t) = b$	$\frac{du(x_\ell,t)}{dx} = b$	$u(x_\ell,t) + \frac{du(x_\ell,t)}{dx} = b$	$a, b \in \mathbb{R}$

The Neumann boundary conditions considered here will always be homogeneous, $a, b = 0$.

Consider a general second order differential equation with constant coefficients.

$$a\frac{\partial^2 u}{\partial x^2} + 2b\frac{\partial^2 u}{\partial x \partial y} + c\frac{\partial^2 u}{\partial y} + d\frac{\partial u}{\partial x} + e\frac{\partial u}{\partial y} + fu + g = 0 \tag{2.8}$$

The leading high order terms dominate the solution of the 2.8 and hence the rest of the equation will be discarded leaving the principal part [33]:

$$a\frac{\partial^2 u}{\partial x^2} + 2b\frac{\partial^2 u}{\partial x \partial y} + c\frac{\partial^2 u}{\partial y} = 0 \tag{2.9}$$

Rewriting in matrix notation gives

$$a\frac{\partial^2 u}{\partial x^2} + 2b\frac{\partial^2 u}{\partial x \partial y} + c\frac{\partial^2 u}{\partial y} = \partial^T A \partial u \tag{2.10}$$

Where $\partial = \begin{bmatrix} \frac{\partial}{\partial x} \\ \frac{\partial}{\partial y} \end{bmatrix}$, $A = \begin{bmatrix} a & b \\ b & c \end{bmatrix}$ and T denotes the transpose

A PDE of this form can be classified according to the eigenvalues of A, given by

$$det\left[A - \mu I\right] = \mu^2 - (a+c)\mu - (b^2 - ac) = 0$$

Specifically, the value of the discriminant $b^2 - ac$ determines the classification of the PDE.

1. $b^2 - ac < 0$ Elliptic - No real characteristic lines exist.

2. $b^2 - ac = 0$ Parabolic - Characteristic lines are coincident.

3. $b^2 - ac > 0$ Hyperbolic - Two classes of characteristic lines exist [52].

The classification names correspond to the shape of the PDE's "'characteristic curves"', along which the PDE can be reduced to an ODE. Any Parabolic PDE may be expressed in the form of the heat equation with the appropriate change of independent variables [33].

This thesis focuses on the diffusion equation, though the techniques extend to the of linear parabolic PDEs. Most of this work can be extended to nonlinear parabolic systems. The canonical classification (parabolic, hyperbolic,...) or shape of the PDE dictates the applicability of the method for realizing a reduced order model. For example, while a parabolic system allows separation of the eigenvalues into a set of dominant slow modes and an infinite dimensional complement of fast modes, a hyperbolic system has eigenvalues which cluster asymptotically nearly the real axis. It is not clear what modes may be discarded for a hyperbolic system[13]. The method used in section 2.3.2 and section 2.3.3 are not applicable to the hyperbolic case. Therefore the class of dynamical systems must be restricted.

2.2.2 Fourier Spectral Solution

A classical solution to the diffusion PDE is expression of the solution as a linear combination of cosines and sines. The diffusion PDE is solved assuming the function may be solved by separation of variables. For a function $v(x,t)$ the separation of variables means expressing it as

$$v(x,t) = f(t)g(x)$$

Only homogeneous Neumann boundary conditions are considered in the experiment section, therefore only solutions with Neumann boundary conditions will be presented. The Fourier solution to the the 1D diffusion PDE results in a solution of the form

$$u(x,t) = a_0(t) + \sum_{n=1}^{\infty} a_n(t) \cos\left(\frac{n\pi x}{\ell}\right)$$

The diffusion equation in one dimension may be rewritten as

$$\frac{\partial u}{\partial t} - \frac{\partial^2 u}{\partial x^2} = 0 \tag{2.11}$$

$$\frac{\partial u(x=0,t)}{\partial x} = \frac{\partial u(x=\ell,t)}{\partial x} = 0 \tag{2.12}$$

The Laplacian of the 1D diffusion equation is evaluated at the steady state resulting in an ODE with boundary conditions

$$\frac{\partial^2 u}{\partial x^2} = \theta^2 u \tag{2.13}$$

$$\frac{\partial u(x=0,t)}{\partial x} = \frac{\partial u(x=\ell,t)}{\partial x} = 0 \tag{2.14}$$

The general solution to the Laplacian ODE is

$$\frac{\partial u(x)}{\partial x} = -c_1\theta\sin(\theta x) + c_2\theta \tag{2.15}$$

Evaluating 2.15 at the boundaries the eigenvectors are

$$\cos\left(\frac{n\pi x}{\ell}\right), \quad n = 1, 2, 3... \tag{2.16}$$

The particular solution of the Laplacian ODE subject to boundary conditions is

$$u(x) = a_0 + \sum_{n=0}^{\infty} a_n \cos(\frac{n\pi x}{\ell}) \tag{2.17}$$

$$a_0 = \frac{1}{\ell}\int_0^{\ell} u(x)dx \tag{2.18}$$

Where each a is a Fourier coefficient determining the weight of the eigenfunction. The method to find the Fourier coefficients may be found in [46]. The Fourier analysis thus gives an analytical solution to the diffusion equation. The analytical solution here may be truncated to a basis of finite size but with increasing error as the truncation order decreases. Analytic solutions of the 1D and 2D diffusion equation will be useful for comparison to solutions using empirical bases. The solution for the 2D diffusion equation with Neumann boundary conditions is given by the Fourier double cosine

series and simply stated

$$u(x,y) = a_{00} + \sum_{m=0}^{\infty}\sum_{n=0}^{\infty} a_{mn}\cos\left(\frac{m\pi x}{\ell_1}\right)\cos\left(\frac{n\pi y}{\ell_2}\right) \tag{2.19}$$

$$a_{00} = \frac{1}{\ell_1\ell_2}\int_0^{\ell_1}\int_0^{\ell_2} u(x,y)dxdy \tag{2.20}$$

2.2.3 Numerical Approximation

The solution of the diffusion PDE may also be found utilizing numerical methods. Two methods are reviewed. First the finite difference approximation is found. This is useful as it is used in section 3.3.1 to compare performance of the state estimator using a reduced order model with an estimator using a high dimension finite difference solution of the diffusion PDE in one dimension. Also, the finite difference of the second order partial differential operator is the Laplacian. A numerical approximation for the Laplacian is required for projecting the diffusion PDE onto a finite dimensional basis. Lastly, the finite difference spatial discretization is used in the numerical Method of Lines (MOL); the MOL is used to generate a true solution of the system.

2.2.3.1 Finite Difference Method

The finite difference solution is a simple solution technique which demonstrates a numerical solution to differential equations in a straight forward way. The finite difference method discretizes the spatial domain into a finite number of points where the solution estimate is known. Here the term estimate refers to error caused by discretizing the domain into a finite number of points. The finite difference solution will be derived for the 1D diffusion equation and stated for two dimensions. For simplicity the spatial domain is discretized linearly for the 1D case and as a rectilinear grid in the 2D case. The solution of the diffusion PDE varies in space and time, the time point will be fixed for the derivation of the finite difference formula in space; u is meant to correspond to $u(x)$ which has no variation in time.

The domain of the independent variable 0 to ℓ will be divided into equally sized increments Δx into N spatial grid points.

$$N = \frac{x_\ell - x_0}{\Delta x} + 1$$

The second derivative at point x_i of a function u will be approximated using values of u at

x_i and some neighboring points.

The forward derivative is traditionally expressed as

$$u'(x) = \lim_{h \to 0} \frac{u(x+h) - u(x)}{h}$$

The Taylor expansion of $u(x)$ about point x is give by [121]

$$f(x) = f(x_i) + \frac{du(f_i)}{dx}(x - x_i) + \frac{1}{2}\frac{d^2 f(x_i)}{dx^2}(x - x_i)^2 + \frac{1}{6}\frac{d^3 f(x_i)}{dx^3}(x - x_i)^3 + H.O.T. \tag{2.21}$$

Writing the derivative in a finite difference form may be done using the Taylor expansion

$$u(x_i + \Delta x) = u(x_i) + u'(x_i)\Delta x + \frac{1}{2}u''(x_i)\Delta x^2 + u^3(x_i)\Delta x^3 + H.O.T.$$

Rearranging

$$u'(x) = \frac{u(x + \Delta x) - u(x)}{\Delta x} - \frac{1}{2}u''(x)\Delta x^2 - u^3(x)\Delta x^3 - H.O.T.$$

$$u'(x) = \frac{u(x) - u(x)}{\Delta x} \quad \underbrace{-\frac{1}{2}u''(x)\Delta x^2 - u^3(x)\Delta x^3 - H.O.T.}_{\mathbf{O}(\Delta x^2)} \tag{2.22}$$

$$u'(x) = \frac{u(x_{i+1}) - u(x_i)}{\Delta x} + \mathbf{O}(\Delta x^2) \tag{2.23}$$

where $\mathbf{O}(\Delta x^2)$ indicates the magnitude of the error can be bounded by a term that decreases proportionally to Δx^2 as Δx becomes small.

Similarly the backward difference is

$$u'(x) = \frac{u(x_i) - u(x_{i-1})}{\Delta x} + \mathbf{O}(\Delta x^2)$$

The second derivative my be found using the Taylor expansion. Consider the Taylor expansion at $u(x_i + \Delta x)$ and $u(x_i - \Delta x)$

$$u(x_i + \Delta x) = u(x_i) + u'(x_i)\Delta x + \frac{1}{2}u''(x_i)\Delta x^2 + \mathbf{O_1}(\Delta x^3)$$

$$u(x_i - \Delta x) = u(x_i) - u'(x_i)\Delta x + \frac{1}{2}u''(x_i)\Delta x^2 + \mathbf{O_2}(\Delta x^3)$$

add the two

$$u(x_i + \Delta x) + u(x_i - \Delta x) = 2u(x_i) + u''(x_i)\Delta x^2 + \mathbf{O_1}(\Delta x^3) + \mathbf{O_2}(\Delta x^3)$$

Rearranging

$$u''(x_i) = \frac{u(x_i + \Delta x) - 2u(x_i) + u(x_i - \Delta x)}{\Delta x^2} + \mathbf{O}(\Delta x^3) \tag{2.24}$$

The subscript form of the diffusion equation is

$$u_t = \alpha u_{xx}$$

where u varies in both space and time. For a small known change in time Δt the diffusion equation may be written as

$$\frac{u(x_i, t_{\tau+1}) - u(x_i, t_\tau)}{\Delta t} = \alpha \cdot u_{xx}(x_i, t_\tau)$$

using the explicit Euler approximation. The change for a given increment of time is

$$u_t(x_i) = u(x_i, t_{\tau+1}) - u(x_i, t_\tau) = \alpha \Delta t \cdot \ u_{xx}(x_i, t_\tau)$$

substituting the finite difference form of the second derivative the finite difference form of the diffusion equation is

$$u_t(x_i) = \alpha \frac{\Delta t}{\Delta x^2}(u_{x_{i-1}} - 2u_{x_i} + u_{x_{i+1}}) \tag{2.25}$$

The finite difference formula is usually written in a short hand notation where u_i denotes the value of $u(i)$

$$u_t(x_i) = \alpha \frac{\Delta t}{\Delta x^2}(u_{i-1} - 2u_i + u_{i+1})$$

The $(1) - (-2) - (1)$ term in the right hand side of the finite difference equation is often called a stencil. Find the solution may then be found my moving the stencil around the domain and carrying about the operation. Obviously, special consideration needs to be taken when the stencil is on the edge of the boundary of the domain. For the Dirichlet case enforcement of boundary conditions simply requires setting the values at the points x_1 and x_N to a and b, respectively. To properly

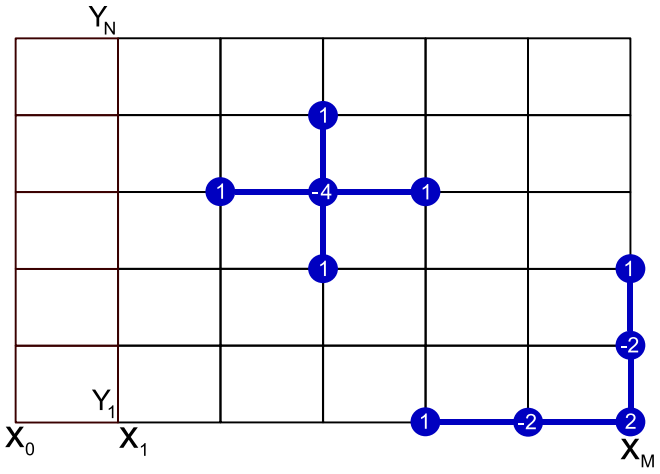

Figure 2.1: Finite difference discretization of a 2D domain. The x axis is discretized into points from x_1 to x_M while the y axis is discretized into points from y_1 to y_N. The points at x_0 are fictitious points outside the real boundary of the system.

enforce Neumann boundary conditions, fictitious points must be placed at x_0 and x_{N+1} (see figure 2.2.3.1) since the second order centered finite difference stencil for the first derivative would not be applicable at x_1 and x_N. The finite difference formula is then solved at the boundary enforcing the boundary condition. The solution for the a homogeneous Neumann condition at x_1 will be solved and the solution at x_N stated.

$$u_t(x=0) = \frac{\Delta t}{\Delta x^2}(u_{i-1} - 2u_i + u_{i+1}) = 0$$

$$u_t(x=0) = \frac{\Delta t}{\Delta x^2} 2(u_{i+1} - u_i) \tag{2.26}$$

the second Neumann boundary condition is

$$u'(x=\ell) = \frac{1}{\Delta x^2} 2(u_{i-1} - u_i) \tag{2.27}$$

It is simple to extend the finite difference formula to the 2D case

$$u_t(i,j) = \alpha \frac{\Delta t}{\Delta x^2}(u_{i-1,j} - 2u_{i,j} + u_{i+1,j}) + \alpha \frac{\Delta t}{\Delta y^2}(u_{i,j-1} - 2u_{i,j} + u_{i,j+1}) \tag{2.28}$$

The results of 2.26 and 2.27 may be applied to enforcement of Neumann boundary conditions

in the 2D case just as 2.25 to the second central difference in two dimensions in 2.28. The difference equations enforcing the boundary conditions are stated:

$$
\begin{aligned}
u_t(i,j) &= \alpha\tfrac{\Delta t}{\Delta x^2}(u_{i-1,j} - 2u_{i,j} + u_{i+1,j}) + \alpha\tfrac{dt}{\Delta y^2}2(2u_{i,j+1} - u_{i,j}) && 0 < i < \ell_1 && j = 0\\
u_t(i,j) &= \alpha\tfrac{\Delta t}{\Delta x^2}(u_{i-1,j} - 2u_{i,j} + u_{i+1,j}) + \alpha\tfrac{dt}{\Delta y^2}2(u_{i,j-1} - u_{i,j}) && 0 < i < \ell_1 && j = \ell_2\\
u_t(i,j) &= \alpha\tfrac{\Delta t}{\Delta x^2}2(u_{i+1,j} - u_{i,j}) + \alpha\tfrac{dt}{\Delta y^2}(u_{i,j-1} - 2u_{i,j} + u_{i,j+1}) && i = 0 && 0 < j < \ell_2\\
u_t(i,j) &= \alpha\tfrac{\Delta t}{\Delta x^2}2(u_{i-1,j} - u_{i,j}) + \alpha\tfrac{dt}{\Delta y^2}(u_{i,j-1} - 2u_{i,j} + u_{i,j+1}) && i = \ell_1 && 0 < j < \ell_2\\
u_t(i,j) &= \alpha\tfrac{\Delta t}{\Delta x^2}2(u_{i+1,j} - u_{i,j}) + \alpha\tfrac{dt}{\Delta y^2}2(u_{i,j+1} - u_{i,j}) && i = 0 && j = 0\\
u_t(i,j) &= \alpha\tfrac{\Delta t}{\Delta x^2}2(u_{i+1,j} - u_{i,j}) + \alpha\tfrac{dt}{\Delta y^2}2(u_{i,j-1} - u_{i,j}) && i = 0 && j = \ell_2\\
u_t(i,j) &= \alpha\tfrac{\Delta t}{\Delta x^2}2(u_{i-1,j} - u_{i,j}) + \alpha\tfrac{dt}{\Delta y^2}2(u_{i,j+1} - u_{i,j}) && i = \ell_1 && j = 0\\
u_t(i,j) &= \alpha\tfrac{\Delta t}{\Delta x^2}2(u_{i-1,j} - u_{i,j}) + \alpha\tfrac{dt}{\Delta y^2}2(u_{i,j-1} - u_{i,j}) && i = \ell_1 && j = \ell_2
\end{aligned}
$$

The explicit Euler solution method described in this section is subject to a limited stability region. A relation between the size of the time step and spatial discretization must be met to ensure stable integration. The relation is defined by the Courant-Friedrichs-Lewys (CFL) condition number. The following ratio must be satisfied [52].

$$\frac{dt}{\Delta x^2} \leq \frac{1}{2}$$

2.2.3.2 Discrete Laplacian

The discrete Laplacian is required for model reduction later. The finite difference formulas derived in section 2.2.3.1 are directly applicable. The Laplacian of a function u in the spatial domain $x \in \Omega$ is

$$\nabla^2 u = \frac{\partial^2 u}{\partial x^2}$$

Unlike the explicit Euler method for solving a system with boundary conditions, taking the discrete Laplacian of a discrete field is not subject to a set of given boundary conditions. The edges of the field must be found using forward and backward differences. For the 1D case the second forward difference is given by taking the derivative of the first forward difference at two adjacent points.

$$u_i = \frac{\frac{(u_{i+2}-u_{i+1})}{\Delta x} - \frac{(u_{i+1}-u_i)}{\Delta x}}{\Delta x}$$

$$
\begin{array}{rcll}
\nabla^2 u_i & = & \frac{1}{\Delta x^2}(u(x_i+h) - 2u(x_i) + u(x_i-h)) & 0 < i < \ell \\
& = & \frac{1}{\Delta x^2}(u_i - 2u_{i+1} + u_{i+2}) & i = 0 \\
& = & \frac{1}{\Delta x^2}(u_i - 2u_{i-1} + u_{i-2}) & i = \ell
\end{array}
$$

Table 2.1: 1D discrete Laplacian formulas

$$
\begin{array}{rllll}
\nabla^2 u_{i,j} & = \frac{1}{\Delta x^2}(u_{i-1,j} - 2u_{i,j} + u_{i+1,j}) + \frac{1}{\Delta y^2}(u_{i,j-1} - 2u_{i,j} + u_{i,j+1}) & 0 < i < \ell_1 & 0 < j < \ell_2 \\
& = \frac{1}{\Delta x^2}(u_{i-1,j} - 2u_{i,j} + u_{i+1,j}) + \frac{1}{\Delta y^2}(u_{i,j} - 2u_{i,j+1} + u_{i,j+2}) & 0 < i < \ell_1 & j = 0 \\
& = \frac{1}{\Delta x^2}(u_{i-1,j} - 2u_{i,j} + u_{i+1,j}) + \frac{1}{\Delta y^2}(u_{i,j} - 2u_{i,j-1} + u_{i,j-2}) & 0 < i < \ell_1 & j = \ell_2 \\
& = \frac{1}{\Delta x^2}(u_{i,j} - 2u_{i+1,j} + u_{i+2,j}) + \frac{1}{\Delta y^2}(u_{i,j-1} - 2u_{i,j} + u_{i,j+1}) & i = 0 & 0 < j < \ell_2 \\
& = \frac{1}{\Delta x^2}(u_{i,j} - 2u_{i-1,j} + u_{i-2,j}) + \frac{1}{\Delta y^2}(u_{i,j-1} - 2u_{i,j} + u_{i,j+1}) & i = \ell_1 & 0 < j < \ell_2 \\
& = \frac{1}{\Delta x^2}(u_{i,j} - 2u_{i+1,j} + u_{i+2,j}) + \frac{1}{\Delta y^2}(u_{i,j} - 2u_{i,j+1} + u_{i,j+2}) & i = 0 & j = 0 \\
& = \frac{1}{\Delta x^2}(u_{i,j} - 2u_{i+1,j} + u_{i+2,j}) + \frac{1}{\Delta y^2}(u_{i,j} - 2u_{i,j-1} + u_{i,j-2}) & i = 0 & j = \ell_2 \\
& = \frac{1}{\Delta x^2}(u_{i,j} - 2u_{i-1,j} + u_{i-2,j}) + \frac{1}{\Delta y^2}(u_{i,j} - 2u_{i,j+1} + u_{i,j+2}) & i = \ell_1 & j = 0 \\
& = \frac{1}{\Delta x^2}(u_{i,j} - 2u_{i-1,j} + u_{i-2,j}) + \frac{1}{\Delta y^2}(u_{i,j} - 2u_{i,j-1} + u_{i,j-2}) & i = \ell_1 & j = \ell_2
\end{array}
$$

Table 2.2: 2D discrete Laplacian formulas

The forward difference is

$$u_i' = \frac{1}{\Delta x^2}(u_i - 2u_{i+1} + u_{i+2}) \tag{2.29}$$

Similarly the second backward difference is

$$u_i' = \frac{1}{\Delta x^2}(u_i - 2u_{i-1} + u_{i-2}) \tag{2.30}$$

The formulas for the dicrete Laplacian in 1D and 2D are given in tables 2.1 and 2.2 respectively.

2.2.3.3 Numerical Method of Lines

The numerical Method of Lines is a PDE solution technique which treats a PDE as a system of ordinary differential equations which can be solved using standard ODE solvers. The advantage of using the MOL is utilization of well documented ODE solvers such as Matlab Runge-Kutta solver `ode45` or stiff solver `ode15s`. The MOL discretizes all but one independent variable; typically the spatial domain is discretized and the temporal is not. Figure 2.2 depicts the state trajectories for a 1D diffusion equation discretized into a system of ODEs. The system of ODEs could be solved using standard analytical means making it a semi-analytical technique. Rather than using analytical techniques a numberical ODE solver will be used. The finite difference approximation for the second derivative 2.25 is used to discretize the spatial domain. The 1D diffusion PDE 2.5 is then replaced

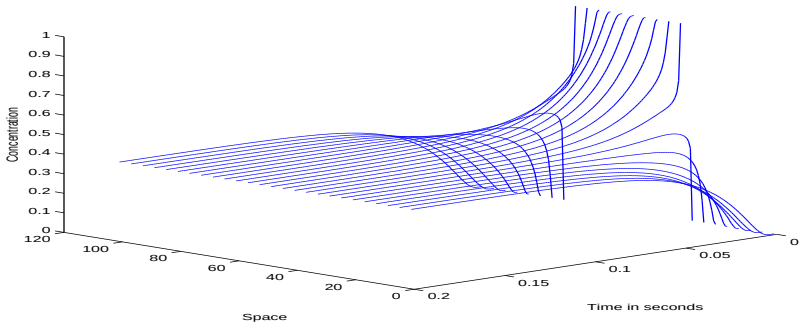

Figure 2.2: Solution to the 1D diffusion equation. Each line represents the state evolution for that particular point in the spatial discretizaton.

with functions

$$u(x,t) = u_i(t) \quad i = 1, 2, ..., M \tag{2.31}$$

subject to initial and boundary value conditions

$$u(x, t = 0) = f(x) \quad u(x = 0, t) = g_1(t) \quad u(x = M, t) = g_2(t) \tag{2.32}$$

More clearly the system of ODEs may be written

$$\frac{\partial u_i}{\partial t} = \alpha \frac{u_{i+1} - 2u_i + u_{i-1}}{\Delta x^2} \quad i = 1, 2, ..., M \tag{2.33}$$

The system of coupled ODEs may now be integrated using a numerical integrator. A stiff ODE integrator is recommended even for coarse spatial discretizations. Stiffness of an equation refers to presence of dynamics with different time scales in the solution requiring small time steps to ensure stability of the solution. As the discretization is refined the system of ODEs becomes stiffer making non-stiff solvers ineffective at producing a solution is reasonable time [116]. One eigenvalue is near the origin with magnitude $\lambda_1 \approx -\pi^2$ for any size of the spatial increment. The largest eigenvalue is $\lambda_m \approx -4/\Delta x^2$. The ratio of these two indicate the stiffness: $4/\pi^2 \Delta x^2$. As Δx gets small the stiffness becomes very large [78].

2.3 Reduced Order Model (ROM)

The state estimator is built using a finite dimensional model of the diffusion process. The diffusion process is naturally distributed and described by an infinite dimensional system. Using numerical techniques the diffusion equation can be solved as a high but finite dimensional system. Unfortunately brute force numerical methods do not lend themselves to practical state estimator or control synthesis. A comparison of the (i) true system state, (ii) linear interpolation of sixteen sensors and (iii) a reduced order model estimating state from five sensors is shown in figure 2.3. Simply linearly interpolating between sensor points yields a poor estimate of state while the estimator based on a reduced order model performs much better. The order of the diffusion equation will be reduced using the Karhunen-Loéve-Galerkin (KLG) model order reduction technique for use in construction the state estimator.

The Karhunen-Loéve expansion decomposes observations of a system into a set of principle mode shapes; the set of observations is the ensemble. The ensemble must include all dynamic behavior the reduced order model is expected to reproduce which may be composed from numerical simulations or measurements of an experiment. For example, time instances taken from a numerical solution to the diffusion equation satisfying a given initial condition with Neumann boundary conditions could be used as the ensemble. The principle mode shapes are found using Karhunen-Loéve (KL) decomposition and the linear Galerkin method is used to project the system onto the KL basis. The reduced order model may then be used to simulate or predict system response similar to that in the input ensemble. If the reduced order model is given dissimilar conditions such as an initial condition far different from that of the input ensemble or a system with different boundary conditions the approximation of the original system given by the reduced order model will be poor.

The Karhunen-Loeve-Galerkin method has been applied to many problems. A review of reduced order model literature with a focus on the KLG method will be presented. The tools for forming the reduced order model will then next be shown. The theoretical framework for decomposing the input ensemble into a set of empirical modes using the Karhunen-Loéve expansion will be derived. Next the linear Galerkin method will be derived for projecting the system dynamics onto a set of basis functions. The Karhunen-Loéve expansion and Galerkin Method will then be shown to yield a finite set of ODEs forming the reduced order model.

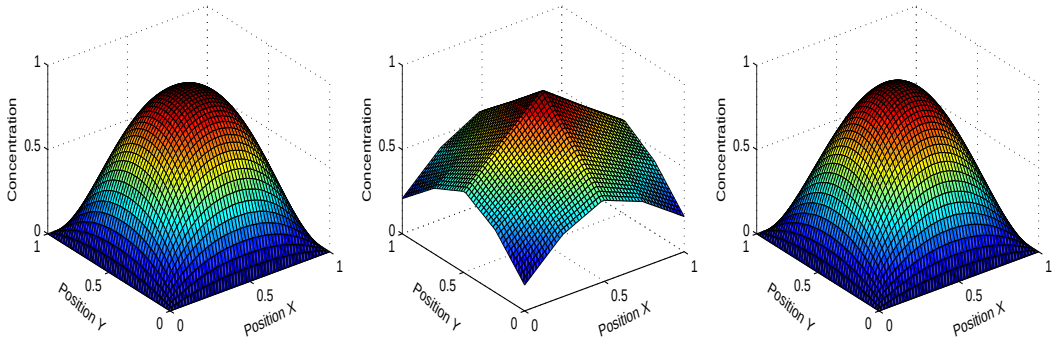

Figure 2.3: Left: True solution of the 2D diffusion equation with unitary diffusion coefficient at 25ms. Middle: Linearly interpolated state from sixteen sensors. Right: State estimate from five sensors using a reduced order model and a Kalman filter.

2.3.1 ROM Literature Review

The Karhunen-Loéve expansion is known by many names depending on the respective field of application, most notable names are the Principal Orthogonal Decomposition (POD), Principal Components Analysis (PCA), singular value decomposition and the Hotelling Transform. Likewise a multiplicity exists in the name of the basis functions obtained through the modal decomposition: empirical modes, principal orthogonal modes and empirical orthogonal functions (eof) [57]. Several researchers independently introduced the Karhunen-Loéve decomposition: Pearson [102], Hotelling [59], Kosambi [72], Loéve [80], Karhunen [63], Pougachev [106] and Obukhov [96].

The primary use of the Karhunen-Loéve procedure bas been for complexity reduction. Early application of the KLE was in the field of fluid dynamics in analysis of turbulent flows for coherent structures. The idea of coherent structures in turbulent flows was first proposed by Liepmann [79] and then subsequently used by Townsend [125]. A coherent structure is defined as a spatial feature in the flow which have a number of characteristic appearance over an appreciable amount of time. [17]. Application of the KLE in the area of turbulence was first used by Lumley [81].

The Karhunen-Loéve procedure is pervasive and has found application in more areas than analysis of turbulent flows. Some limited use has been found in the area of data and image compression. Andrews et. al proposed the the Karhunen-Loéve transform as a data compressor [6]. The Karhunen-Loéve transform is used to generate a data dependent autocorrelation based compression of the data. While the compression is optimal for the data a significant negative is the autocorrelation matrix must be available to the decoder. For data sources that are non-stationary

the autocorrelation will vary requiring transfer of the autocorrelation tensor resulting in an impractical compression technique in many circumstances [115]. The compression made available by KL expansion has also found a niche in facial recognition. Here, an ensemble of training images is used to produce the autocorrelation matrix and thusly the eof. Images in the original ensemble may be represented as a linear combination of the eof. Kirby and Sirovich used the eof from KL expansion to represent faces not in the training set [68]. Turk and Pentland built on the work of Kirby and Sirovich developing a facial recognition algorithm using the eof weights to measure the closeness of a face with those in the training set [126].

Some early investigation of control using modal approximations of distributed parameter systems was performed by Balas. Balas examined a truncated modal approximation of a linear diffusion process and theoretical design of a modal controller. The effect of the truncated modes receiving 'spillover' control energy is proven to not cause divergence undesirably affect the dissipative characteristic of the system [14]. Balas also proved a stable finite dimensional controller for the Galerkin approximation of a distributed parameter system exists [15].

Controllers using KLG approximations to linear systems have been made by several researchers. Kunisch and Volkwein synthesize a closed loop suboptimal feedback controller for the Burgers' equation using a reduced order model formed from a Galerkin approximation using modes recovered from the Karhunen-Loéve expansion. Park and Cho investigate Karhunen-Loeéve Galerkin approximations to the nonlinear heat equation. Effects of model order, ensemble size, varying boundary values on error are found [101].Chen and Chang develop a control theory for nonlinear systems with unknown dynamics for systems with a partitionable eigenspectrum with applications to chemical systems. The Karhunen-Loéve-Galerkin methodology is used in development of the nonlinear feedback control law [27].

Many extensions of the KLG procedure have been proposed. Graham and Kevrekidis modify the Karhunen-Loéve decomposition to accommodate non-uniform sampling of the input ensemble and weighted ensemble averages to emphasize events or structures that are localized in space or time [48]. Rowley and Mardsen extended the Karhunen-Loéve-Galerkin procedure to accommodate traveling waves. [114]. Roweley et al. extend the previous work for self-similar dynamic systems [113]. Rambo used a flux matching procedure to accommodate inhomogeneous boundary conditions for a KLG reduced model[110]. Applying the Karhunen-Loéve expansion to partial data is addressed by Everson and Sirovich [36].

For nonlinear systems the model produced using the linear Galerkin method may not capture satisfactory dynamics. A variation on the linear Galerkin method is the nonlinear Galerkin method [83]. The linear Galerkin method projects the dynamic system on a finite set of basis functions while the nonlinear Galerkin method projects the system on an inertial manifold. An inertial manifold is a positively invariant Lipschitz manifold which exponentially attracts all state trajectories to the manifold in finite time [39]. The dynamics of the dynamic system reduce to ODEs on the inertial manifold. ODE analysis techniques applied to the ODEs provide accurate analysis of the PDE system. Some systems have inertial manifolds which may be proven using existence proofs. For systems which are proven to have an inertial manifold results of the existence proof does not produce the inertial manifold itself. Approximate inertial manifolds (AIM) have been proposed which attract the state trajectories exponentially in finite time [124]. A sampling of AIM techniques will be stated, an extensive review of model reduction using AIMs and comparison with Karhunen-Loéve decomposition & flat Galerkin projection see the Shvartsman and Kevrekidis review paper [117].

Christofides and associates have proposed controllers using combinations of Karhunen-Loéve expansion, AIMs and Galerkin's method. Systems governed by the diffusion-convection-reaction equations (used in *in silico* models) which are parabolic PDE systems which may separated into fast and slow modes. Nonlinear finite-dimensional models are developed and a nonlinear control law developed [29]. They have also applied this methodology to systems with time dependent spatial domains for linear Galerkin and nonlinear Galerkin methods and subsequently synthesizing a robust controller for the diffusion-convection-reaction system with uncertainty [8] [10] [9]. Controllers have also been synthesized for the one dimensional Burgers equation and the 2D Navier-Stokes equation [11]. They have also synthesized a nonlinear controller for the spatially nonlinear system describing a rapid thermal chemical vapor deposition process. [12] [13]. A nonlinear controller for a particle size distribution process governed by first order hyperbolic and integro-differential equations was synthesized as well [28].

The Karhunen-Loéve-Galerkin formulation is only one example. Several other model reduction techniques exist worth mentioning. For pure spectral techniques (as opposed to pseudospectral collocation techniques) other basis sets may be used. Building an optimal set of orthogonal basis functions using empirical data via the Karhunen-Loéve expansion is limited to recreating initial conditions which were observed in the input ensemble. Fourier cosine or sine bases are applicable

to periodic boundary conditions. Chebyshev Legendre polynomials, Laguerre series and Chebyshev series may also by used provided by satisfy the requirements of the projection technique [47].

The balanced truncation proposed by Moore has been used with Karhunen-Loéve decomposition to form a reduced model from input-output data [87]. The controllability and observability grammians are computed and used to find a coordinate transformation which balances the grammians so they are diagonal and equal. States which are not affected much by input have little effect on output in in the balanced coordinates and subsequently truncated. While the results are not guaranteed to be optimal the error bounds of the reduced model are known. The Galerkin projection is then used to find an empirical balanced realization for the linear [128] [112] or nonlinear system [74].

The Tau approximation proposed by Lanczos is similar to the Galerkin method. The orthonormal basis set for the Tau approximation is not required to satisfy the boundary conditions as the Galerkin procedure is. An additional set of functions are required to enforce the boundary conditions which may be (in)homogeneous [47]. For an overview of the Tau method see [97], [47]; Some examples are provided in [47].

Wavelet-Galerkin methods have been proposed as a solution technique to partial differential equations motivated by ability to describe multiple scales of resolution [3] [107] [18]. Wavelet-Galerkin solvers have been shown to produce computationally efficient and accurate results in comparison to finite element approximations of PDE's. Qian and Weiss investigated the wavelet-Galerkin method for nonlinear PDEs with periodic boundary conditions [107]. Beylkin and Keiser developed computation algorithms for solving the heat equation, Burgers' equation and the generalized Burgers' equation with the wavelet-Galerkin method [18]. Some use of the wavelet-Galerkin method has been found in system identification [45] [67] [24] and control [64].

2.3.2 Karhunen-Loéve Expansion

The modes found using the Karhunen-Loéve expansion will be the basis set for the reduced order model. At each time step the reduced order system will be expressed as a linear combination of the empirical modes. The underlying dominant dynamics of the infinite dimensional system are projected onto the finite basis set found from the Karhunen-Loéve expansion.

Suppose some set of functions $U = \{u_1,\ u_2,\ ...,\ u_M\}$ with multiplicity M belong to the infinite-dimensional $\mathcal{L}^2(\Omega)$ Hilbert space $\mathcal{H}$. Each function $u_i = u_i(x)$ is a spatial function that

defines a scalar field in the domain $x \in \Omega$ describing the system at each observed time increment m. This set of functions are found through numerical simulations or physical experiments and will be used to find the empirical modes [57].

The Karhunen-Loéve Expansion allows expression of a function as a linear combination of eigenfunctions in the form of the expansion

$$u(x,t) = u_0(x,t) + \sum_{n=1}^{\infty} a_n \phi_n(x) \tag{2.34}$$

Where each $\phi_n(x)$ is a basis function satisfying the boundary conditions. The $u_0(x,t)$ is a source function satisfying time varying or inhomogeneous boundary conditions. Interest is limited to static homogeneous boundary conditions in this work. The weighting coefficients $a_n(t)$ will be found later via a system of ordinary differential equations for a system similar to 2.34 which is finite dimensional and varies in time.

The Hilbert space has the inner product

$$(f,g) = \int_{\Omega} f(x)g(x)dx$$

and the induced $\mathcal{L}^2$-norm

$$\|f\| = (f,f)^{\frac{1}{2}}$$

It is desired to have the best projection of $U = \{u_1(x),\ u_2(x),\ ...,\ u_n(x)\}$ onto a basis $\Phi = \{\phi_1,\ \phi_2,\ ...,\ \phi_n\}$ for $\mathcal{H}$. The average projection of U onto Φ is

$$\max_{\Phi \in \mathcal{L}^2(\Omega)} \frac{\langle |(U,\Phi)^2| \rangle}{\|\Phi\|^2} \tag{2.35}$$

where $\langle \alpha_i \rangle = \frac{1}{n} \sum \alpha_i$ is an averaging operation and $\| \cdot \|$ is the modulus. To find the optimal basis the average projection needs to be extremized. Maximizing 2.35 is tantamount to minimizing the projection error. Extremizing the numerator of 2.35 with the constraint $\|\Phi\|^2 = 1$ is a calculus of variations problem [57], with cost functional

$$J[\Phi] = \langle |(U,\Phi)|^2 \rangle - \lambda(\|\Phi\|^2 - 1)$$

The λ is a Lagrange multiplier. The solution of the variational problem must satisfy [57]

$$\int_{\Omega} \langle U(x), U(x') \rangle \Phi(x') dx' = \lambda \Phi(x). \tag{2.36}$$

The autocorrelation function is defined as the kernel function of the integral transform in the previous equation.

$$R(x, x') = \langle U(x), U(x') \rangle$$

The $u_m(x)$ functions are system snapshots. The system snapshots will be discretized observations of the system. The domain of x discretized into k values. The $u_m(x)$ continuous function is then replaced by the vector $\mathbf{u}_m(x)$ where the boldface indicates vector or matrix. The autocorrelation function is then replaced by a tensor product [57]

$$\mathbf{R} = \langle \mathbf{U} \otimes \mathbf{U}^* \rangle$$

where $(\cdot)^*$ denotes the complex conjugate The eigenvectors of the $\mathbf{R}$ matrix correspond to the principal components of ensemble samples $u_m(x)$.

The maximum of 2.35 will exist for the operator $\Re$ given it is compact self-adjoint [57]. The integral 2.36 may now be written as the eigenvalue-eigenvector problem

$$\Re \Phi = \lambda \Phi$$

Given the set of empirical orthogonal basis functions φ composed of the set of functions $\{\phi_1, \phi_2, \phi_3, ..., \phi_n\}$, the energy of each eigenvector $\lambda_p = \langle |(u_p(x), \Phi)|^2 \rangle$ may be written as

$$E_p = \frac{\lambda_p}{\sum_{j=1}^{m} \lambda_j}$$

The total energy retained by n modes is

$$E = \sum_{p=1}^{n} E_p$$

The system must retain the 99.9% of the energy given by the largest eigenvalues, the associated eigenvectors form the truncated basis.

2.3.3 Galerkin Projection

The linear Galerkin method seeks to find an optimal projection of a function onto a finite set of basis functions. The system $u(x,t)$ may be written as the series expansion

$$u(t,x) = \sum_{n=1}^{N} a_n(t)\phi_n(x)$$

Where $a_n(t)$ are coefficients which serve as weights for a linear combination of the basis set $\phi_n(x)$. The dynamics of the coefficients $a_n(t)$ are found using the Galerkin method; they are the dynamics of the reduced-order model. The Galerkin method has no knowledge of the system boundary conditions and requires that the basis functions used for the projection independently satisfy the boundary conditions [47] [57]. The test functions used may be any set of orthonormal functions satisfying the boundary conditions such as Chebyshev polynomials, Karhunen-Loéve empirical orthogonal functions, Fourier series, etc.

The 1D diffusion system in 2.4 is rewritten as

$$\frac{du}{dt} = D\nabla^2 u = Au$$

$$\frac{du}{dt} - Au = 0 \tag{2.37}$$

where $A(\cdot) = D\nabla^2(\cdot)$ is the spatial operator. The residual error of the approximate system from the full rank system is defined as

$$r(t,x) = \frac{\partial u}{\partial t} - A(u)$$

It is desired that the residual be zero, however, this is not possible. The objective is to obtain a system which is realizable in real time, hence the number of basis functions must be finite. The set of basis functions is truncated, which forms a basis which does not span the entire subspace but still describes the underlying system sufficiently. The residual may be made orthogonal to the truncated basis to minimize the error [57].

$$(r(t,x), \phi_n(x)) = 0 \quad n = \{1,\ ...,\ N\} \tag{2.38}$$

The solution u of the system is expressed as a truncated series.

$$u(t,x) = \sum_{n=1}^{N} a_n(t)\phi_n(x) \tag{2.39}$$

Substituting 2.39 into 2.37 expresses the residual in terms of a series expansion

$$\begin{aligned} r(t,x) &= \frac{\partial}{\partial t}\sum_{n=1}^{N} a_n(t)\phi_n(x) - A\left(\frac{\partial}{\partial t}\sum_{m=1}^{N} a_m(t)\phi_m(x)\right) && (2.40)\\ &= \sum_{n=1}^{N} \dot{a}_n(t)\phi_n(x) - A\left(\sum_{m=1}^{N} \dot{a}_m(t)\phi_m(x)\right) && (2.41) \end{aligned}$$

The error must now be orthogonalized with respect to the basis functions [92], i.e. ($r(t,x), \phi_i(x)$=0). Then,

$$\begin{aligned} (r(t,x),\phi_i(x)) &= \int_\Omega r(t,x)\phi_i(x)dx && (2.42)\\ &= \int_\Omega \left[\sum_{n=1}^{N} \dot{a}_n(t)\phi_n(x) - A\left(\sum_{m=1}^{N} \dot{a}_m(t)\phi_m(x)\right)\right]\phi_i(x)dx && (2.43)\\ &= \sum_{n=1}^{N} \dot{a}_n(t)\int \phi_n(x)\phi_i(x) - \int_\Omega A\left(\sum_{m=1}^{N} \dot{a}_m(t)\phi_m(x)\right)\phi_i(x)dx && (2.44)\\ &= \dot{a}_i(t) - \int_\Omega A\left(\sum_{m=1}^{N} \dot{a}_m(t)\phi_m(x)\right)\phi_i(x)dx && (2.45)\\ &= 0 && (2.46) \end{aligned}$$

Thus, the error will be orthogonal if [93]

$$\dot{a}_i(t) = \int_\Omega A\left(\sum_{m=1}^{N} \dot{a}_m(t)\phi_m(x)\right)\phi_i(x) \quad i = 1, ..., N \tag{2.47}$$

These ODEs describe the dynamics of the coefficients of the basis.

2.3.4 Finite Dimensional Model

The Karhunen-Loéve and Galerkin methods will be used together to form the reduced order model. The Galerkin projection specific to the diffusion equation is developed. The finite dimensional model employed will use the empirical modes recovered using the Karhunen-Loéve expansion and

application of the linear Galerkin method.

The input ensemble of M observations is mean centered. The modified ensemble is

$$v_m = u_m - \bar{u}$$

where the mean is given by

$$\bar{u} = \frac{1}{M} \sum_{m=1}^{M} u_m$$

The spatial operator for the 1D diffusion equation may then be rewritten

$$\frac{\partial v}{\partial t} = A(v) = \nabla^2 (u + \bar{u})$$

substituting into 2.47

$$\dot{a}_i(t) = \sum_{j=1}^{N} a_j(t) \int_\Omega \phi_i(x) \nabla^2 \phi_j(x) dx + \int_\Omega \nabla^2 \bar{u}(x) \phi_i(x) dx \quad i = 1, .., N \tag{2.48}$$

Applying the Galerkin method to $(\phi_i(x), I(x))$ instead of $(r(t,x), \phi_i(x))$ gives the initial conditions for the boundary value problem

$$a_i(0) = (\phi_i(x), I(x)) = \int_\Omega u(x,0) \phi_i(x) dx \quad i = 1, .., N \tag{2.49}$$

resulting in a system of ODEs of the form

$$\dot{a}(t) = \Gamma a(t) + b \tag{2.50}$$

where

$$\Gamma_{i,j} = \int_\Omega \phi_i(x) \nabla^2 \phi_j(x) dx \tag{2.51}$$

and

$$b_i = \int_\Omega \nabla^2 \bar{u}(x) \phi_i(x) dx \tag{2.52}$$

Once the system is solved and the state vector $a_n(t)$ is recovered. The approximate system

$\bar{u}(t,x)$ of $u(t,x)$ takes the form

$$\hat{u}(t,x) = \bar{u} + \sum_{n=1}^{N} a_n(t)\phi(x)$$

2.4 Kalman Filter

The Kalman filter is the tool that will be used to estimate state. Essentially the filter balances a prediction based on a system model and the measurents from the sensors to provide an optimal estimate. The diffusion process is modeled using the reduced-order model introduced in the previous section. Specifically the solution is represented as a linear combination of fixed basis functions

$$\hat{u}(t,x) = \bar{u} + \sum_{n=1}^{N} a_n(t)\phi(x)$$

and the coefficients evolve in time according to

$$\dot{a}(t) = \Gamma a(t) + b$$

where Γ and b are given by equations 2.51 and 2.52. The observation matrix C for the reduced-order model is given by

$$C = \begin{bmatrix} \phi_1(x_1) & \phi_2(x_1) & \cdots & \phi_N(x_1) \\ \phi_1(x_2) & \phi_2(x_2) & \cdots & \phi_N(x_2) \\ \vdots & \vdots & \ddots & \vdots \\ \phi_1(x_p) & \phi_2(x_p) & \cdots & \phi_N(x_p) \end{bmatrix}$$

It seems a simple solution is to use the sensor data and a pseudo inverse to recover the weights and subsequently apply to the empirical functions but doing so makes the estimate subject to sensor and process noise, which may cause the state to vary greatly.

The Kalman filter is a linear recursive optimal estimator. For linear systems true knowledge of state is usually obscured by sensor and process noise. Inaccuracies arise from sensor noise, biases and parametric uncertainty of the system. The filter is recursive in that it only requires the previous system state to make the estimate. The Kalman filter is not merely a data smoother but uses a dynamic model of the system along with the noise properties to estimate state while minimizing the error is statistically minimized. Using knowledge about sensor and process noise properties, sensor measurements are used to estimate the state [85] [51]. The Kalman filter has also been applied to

weakly nonlinear systems [1]. Only linear estimators are considered in this thesis.

Use of Kalman filtering with reduced order models was first applied in meteorological systems for state estimation and data assimilation although it is typical to see high dimensional Kalman filtering [35] and specialized techniques such as ensemble Kalman filters to eliminate expensive matrix inversions or 4D-VAR [61] [62] for large dimensional systems. Use of the latter techniques require supercomputers with hundreds of processing cores and large memory capacities to accommodate models with tens of thousands or millions of state variables [61].

Many relevant examples of Kalman filtering systems described by PDEs arises from meteorological forecasting. Dee used a modified Kalman filter to assimilate meteorological data [31]. Fukumori developed a Kalman filter for some reduced order approximation of the system dynamics. [44]. Pham, et. al design an extended Kalman filter for a system approximated by empirical orthogonal functions that they termed singular evolutive Kalman Filter (SEEK) [104] [94]. Farrell and Ioannou synthesize a Kalman filter for state estimation using a system approximated by balanced truncation of a Karhunen-Loéve-Galerkin reduced order model [37]. Reduced order Kalman filtering has also found use in fluids for design of fluid controllers [16] [58]. Computationally efficient Kalman filtering was also proposed by Gunther, et. al whereby a Fast Fourier Transform and Galerkin method were used fast nonlinear filtering [53]. Kalman filtering has also been applied to sub-optimal state estimation of a multi-resolution model estimated by a wavelet-Galerkin model [122].

The state will be estimated for a dynamic system expressed in state space form

$$\dot{x}(t) = Ax(t) + \eta(t)$$

or written in terms of a state transition matrix in discrete form

$$x_t = \Phi x_{t-1} + \eta_{t-1}$$

with measurement model

$$y(t) = Cx(t) + \xi(t)$$

or in discrete form

$$y_t = Cx_t + \xi_t$$

where ξ and η are zero mean white Gaussian noise terms

$$\eta = \mathcal{N}(0, V_s)$$

$$\xi = \mathcal{N}(0, V_y)$$

The objective of weighting the measured values and predictions made by the system model will be made through a gain factor.

$$\hat{x}_{t,t} = \bar{K}_t \hat{x}_{t,t-1} + K_t y_t$$

The double subscript notation indicates the timepoint and nature of the variable. Subscript $_{t,t}$ or $_t$ denotes current time, $_{t,t-1}$ denotes the prediction made at the last time step and $_{t+1,t}$ denotes the prediction at the current time step.

The error is minimized when the difference of the true and estimated state is orthogonal to the measurement. Writing in terms of the expected value [51]

$$E\langle (x_t - \hat{x}_{t,t}) Y_i^T \rangle = 0 \quad i = 1, 2, ..., m-1 \tag{2.53}$$

$$E\langle (x_t - \hat{x}_{t,t}) Y_m^T \rangle = 0$$

The matrix $Y = [y_1,\ y_2,\ ..,\ y_m]$ is the history of the system observations.

The error is define

$$\tilde{x}_t = x_t - \hat{x}_t$$

By making use of the orthononality principle, uncorrelated noises and several algebraic manipulations, the expected value conditioned on prior measurements becomes [51]

$$E\langle (-\tilde{x}_{t-1,t} + K_t C \tilde{x}_{t-1,t} - K_t \xi_t)(C\tilde{x}_{t-1,t} - \xi_t)^T \rangle$$

The a priori covariance matrix is defined

$$Q_{t,t-1} = E\langle \tilde{x}_{t,t-1} \tilde{x}_{t,t-1}^T \rangle$$

The Kalman gain is then given

$$K_t = Q_{t,t-1}C^T[CQ_{t,t-1}C^T + V_s]$$

The Kalman gain found using a covariance matrix conditioned on the past measurements, it must be corrected and predicted at each time step. Correction of the error covariance may be written [51]

$$Q_{t,t} = E\langle[\tilde{x}_{t,t+1}\tilde{x}_{t,t+1}^T]\rangle$$

Making substitutions and rearranging

$$Q_{t,t} = (I - K_tC)Q_{t,t-1}(I - K_tC)^T + K_tR_tK_t^T$$

Making additional substitutions

$$Q_{t,t} = (I - K_tC)Q_{t,t-1}$$

The covariance prediction is found using the definition of the error and state updates [51]

$$\begin{aligned} Q_{t+1,t} &= E[\tilde{x}_{t,t-1}\tilde{x}_{t,t-1}^T] && (2.54) \\ &= \Phi Q_{t,t}\Phi^T + Q_{t,t} && (2.55) \end{aligned}$$

The Kalman filter estimates state using the algorithm:

1. Calculate Kalman Gain

   $K_t = Q_{t,t-1}C^T[CQ_{t,t-1}C^T + V_s]^{-1}$

2. Update (estimate) state and predictor covariance

   $\hat{x}_{t,t} = \hat{x}_{t,t-1} + K_t[Y_t - C\hat{x}_{t,t-1}]$

   $Q_{t,t} = [I - K_tC_s]Q_{t,t-1}$

3. Predict next state and predictor covariance

   $\hat{x}_{t+1,t} = \Phi\hat{x}_{t,t}$

   $Q_{t+1,t} = \Phi Q_{t,t}\Phi^T + V_y$

4. Repeat above for each time step

2.5 Numerical Implementation

Several tools were presented in the Background chapter but did not address implementation in a numerical computing environment, such as Matlab®. A succinct account of the implementation methodology that is used to conduct numerical studies and the experiment are presented.

2.5.1 Karhunen Loéve Decomposition

The Karhunen-Loéve expansion decomposes a set of discrete observations of the system into the principle modes. The empirical modes are used as the finite basis the system is projected onto. Refer to section 2.3.2 for a theoretical background.

A set of M observations from numerical simulations is collected and used for the input ensemble. The input ensemble U

$$\mathbf{U} = \mathbf{u}(t) = [\mathbf{u}_1, \mathbf{u}_2, \ ..., \ \mathbf{u}_m]^T \in \mathbb{R}^{M \times N}$$

where each $\mathbf{u}_m(x)$ is discretized into N points in space. The input ensemble is mean centered by subtracting off the mean

$$\bar{u} = \frac{1}{M} \sum_{m=1}^{M} \mathbf{u}_m$$

resulting in the mean centered ensemble

$$\mathbf{V} = \mathbf{U} - \bar{\mathbf{u}}$$

$$\mathbf{V} = \mathbf{v}(t) = [\mathbf{v}_1, \mathbf{v}_2, \ ..., \ \mathbf{v}_m]^T$$

The two point correlation function developed in 2.3.2 is now applicable. The covariance matrix

$$\mathbf{C} = \frac{1}{M} \sum_{\Omega} \mathbf{V}\mathbf{V}^T$$

The covariance matrix C has eigenvectors A and associated eigenvalues λ satisfying

$$CA = \lambda A$$

Singular value decomposition of the covariance matrix C is performed to solve the eigenvalue problem

$$C = U\Sigma V^T$$

where Σ are the singular values, U are the left singular vectors and V are the right singular vectors. The Matlab^{TM} SVD routing `svd()` is used for full decomposition while `svds()` is used to find the k largest singular values and vectors. The columns of V correspond to the eigenvectors of C and are the empirical orthogonal functions. The eigenvectors are then normalized as this is required for the Galerkin projection.

For dimensions higher than one each system snapshot in the ensemble will be a matrix rather than a vector. Each snapshot matrix must be reshaped into a vector to apply the Karhunen-Loéve decomposition. For the 2D case discretized into an $i \times j$ rectilinear domain

$$\mathbf{V} = \begin{bmatrix} v^{1,1} & v^{2,1} & v^{3,1} & \dots & v^{i,1} \\ v^{1,2} & v^{2,2} & v^{3,2} & \dots & v^{i,2} \\ v^{1,3} & v^{2,3} & v^{3,3} & \dots & v^{i,3} \\ \vdots & \vdots & \vdots & \ddots & \vdots \\ v^{1,j} & v^{2,j} & v^{3,j} & \dots & v^{i,j} \end{bmatrix} \tag{2.56}$$

$$\Rightarrow \quad \begin{bmatrix} v^{1,1} & v^{2,1} & \dots & v^{i,1} & v^{1,2} & v^{2,2} & \dots & v^{i,2} & v^{1,3} & v^{2,3} & \dots & v^{i,3} & \dots & v^{1,j} & v^{2,j} & \dots & v^{i,j} \end{bmatrix}^T \tag{2.57}$$

The two point correlation matrix C may now be found. The eigenvectors recovered from the SVD must be reshaped from a vector into a 2D matrix.

2.5.2 Galerkin Projection & Reduced Order Model

The Galerkin method projects the diffusion equation onto a finite set of basis functions which satisfy the boundary conditions and define the dynamics of empirical mode coefficients. See sections 2.3.3 and 2.3.4 for theory. The Galerkin projection is tailored to the diffusion equation for the 1D and 2D cases. For the 1D case the coefficient dynamics are

$$\dot{a}_i(t) = \underbrace{\sum_{j=1}^{N} a_j(t) \sum_{\Omega} \phi_i(x) \nabla^2 \phi_j(x) dx}_{\Gamma} + \underbrace{\sum_{\Omega} \nabla^2 \bar{u}(x) \phi_i(x) dx}_{b}$$

where ∇^2 is approximated by the formulas give in tables 2.1 and 2.2.

The matrices Γ and b for the ODE system describing the dynamics of the empirical mode coefficients are then obtained. To perform a simulation of the diffusion process using the reduced order model the Γ and b matrices are used to define a function for use with a numerical ODE integrator. The dynamic system also needs to be expressed as a system transition matrix for the Kalman Filter. Solving 2.50 by variation of parameters gives

$$a(t) = e^{\Gamma t}a(0) + \int_0^t e^{\Gamma(t-\tau)}bd\tau \tag{2.58}$$

where $a(0)$ is the initial condition.

2.5.3 Kalman Filter - Reduced Order Model Formulation

The Kalman filter estimates the state of the system by weighting sensor measurements and predictions given by the system dynamic model. It is assumed the system is sampled at uniform temporal increments and all sensor values are available with neglible delay.

The system model is

$$\begin{aligned} \dot{a} &= \Gamma a + b \qquad a \in \mathbb{R}^N \\ y &= Ca \qquad y \in \mathbb{R}^p \end{aligned}$$

where a is the state of the reduced-order model.

The observation matrix of the R.O.M. is given for an N^{th} order approximation with P sensor locations. The values of x are the points in the domain for which there are sensors placed

$$C_{ROM} = \begin{bmatrix} \phi_1(x_1) & \phi_2(x_1) & \cdots & \phi_N(x_1) \\ \phi_1(x_2) & \phi_2(x_2) & \cdots & \phi_N(x_2) \\ \vdots & \vdots & \ddots & \vdots \\ \phi_1(x_p) & \phi_2(x_p) & \cdots & \phi_N(x_p) \end{bmatrix} \in \mathbb{R}^{p \times M}$$

The observation vector is

$$y = [y_1\ y_2\ ...\ y_p]$$

Where y_i is the observed sensor value at the corresponding point x_i in the domain.

The state covariance is initialized by solving the Ricatti Equation.

$$\dot{Q} = 0 = \Gamma Q + Q\Gamma - QC_s^T V_y^{-1} C_s Q + V_s \tag{2.59}$$

$$Q_{t=0} = Q \tag{2.60}$$

The `care()` Matlab solver routine is used to solve the Ricatti eqation.

The state of the Kalman filter is initialized by finding a minimum norm fit of the basis functions to the sensor values at $t = 0$. A standard Moore-Penrose inverse (denoted by $\dagger$) is used to recover the states.

$$C_s^{\dagger}[y_1\ y_2\ ...\ y_M]^T = [a_1(t=0)\ a_2(t=0)\ ...\ a_N(t=0)]^T$$

Where the $[\bar{a}]$ vector is the state, the weights of that time instant on the modes.

The state transition matrix Φ is the result of the separation of variables solution in 2.58.

$$\Phi = e^{\Gamma t} a_{t,t}$$

The integrand term in 2.58 evaluated only once using `ode45()` owing to the fixed temporal increment.

$$c = \int_0^t e^{\Gamma(t-\tau)} b d\tau$$

The Kalman filter for the reduced-order model is then given

Calculate Kalman Gain	$K_t = Q_{t,t-1} C_s^T [C_s Q_{t,t-1} C_s^T + V_s]^{-1}$
Estimate State	$\hat{a}_{t,t} = \hat{a}_{t,t-1} + K_t[Y_t - C_s \hat{a}_{t,t-1}]$
Output State	$S = \bar{u} + \sum_{n=1}^{N} a_n(t)\phi_n(x)$
Update Covariance Matrix	$Q_{t,t} = [I - K_t C_s] Q_{t,t-1}$
Predict Next State	$\hat{a}_{t+1,t} = \Phi \hat{a}_{t,t} + c$
Predict Next Covariance Matrix	$Q_{t+1,t} = \Phi Q_{t,t} \Phi^T + V_y$

2.5.4 Kalman Filter - Finite Difference Explicit Euler 1D Implementation

The Kalman filter is implemented for the high dimensional system produced by a finite difference discretization of the 1D diffusion equation. The system is assumed to be discretized into M spatial points with P sensors

The system model is

$$\begin{aligned} \dot{x} &= Ax \qquad a \in \mathbb{R}^M \\ y &= Cx \qquad y \in \mathbb{R}^p \end{aligned}$$

The observation matrix is a diagonal matrix given as

$$C_{ee} = \begin{bmatrix} 1_1 & 0 & 0 & 0 & 0 & ... & 0 \\ 0 & 0 & 0 & 0 & 0 & ... & 0 \\ 0 & 0 & 1_2 & 0 & 0 & ... & 0 \\ 0 & 0 & 0 & 1_3 & 0 & ... & 0 \\ 0 & 0 & 0 & 0 & 0 & ... & 0 \\ \vdots & \vdots & \vdots & \vdots & \vdots & \ddots & \vdots \\ 0 & 0 & 0 & 0 & 0 & ... & 1_P \end{bmatrix} \in \mathbb{R}^{p \times M} \tag{2.61}$$

Where each 1_p on the diagonal is some arbitrarily placed measurement sensor at position p in the spatial domain.

The observation vector is given

$$y = [y_1 \; y_2 \; ... \; y_p]^T$$

The state transition matrix is derived from the finite difference equations given in 2.2.3.1. A banded tri-diagonal matrix is formed using the explicit Euler central difference with forward and backward differences enforcing the Neumann boundary conditions for the 1D case.

$$A = \frac{\Delta t}{\Delta x^2} \begin{bmatrix} -2 & 2 & 0 & 0 & \dots & 0 & 0 & 0 & 0 \\ 1 & -2 & 1 & 0 & \dots & 0 & 0 & 0 & 0 \\ 0 & 1 & -2 & 1 & & 0 & 0 & 0 & 0 \\ \vdots & & & & \ddots & & & & \vdots \\ 0 & 0 & 0 & 0 & & 1 & -2 & 1 & 0 \\ 0 & 0 & 0 & 0 & \dots & 0 & 1 & -2 & 1 \\ 0 & 0 & 0 & 0 & \dots & 0 & 0 & 2 & -2 \end{bmatrix}$$

Putting the finite difference implementation into state transition matrix Φ

$$x_{t+1} = Ax_t + x_t$$

$$x_{t+1} = (A + I)x_t$$

$$\Phi = (A + I)$$

The initial state is found by linearly interpolating between sensor measurements for M values given by the measurement vector

$$x_0 = [y_1\ y_2\ ...\ y_M]$$

The state covariance is initialized by solving the algebraic Ricatti Equation as in 2.59 and 2.60.

The Kalman filter for the explicit Euler approximation is given

Calculate Kalman Gain	$K_t = Q_{t,t-1}C_{ee}^T[C_{ee}Q_{t,t-1}C_{ee}^T + V_s]^{-1}$
Estimate State	$\hat{x}_{t,t} = \hat{a}_{t,t-1} + K_t[Y_t - M\hat{x}_{t,t-1}]$
Output State	$S = \hat{x}_{t,t}$
Update Covariance Matrix	$Q_{t,t} = [I - K_tC_s]Q_{t,t-1}$
Predict Next State	$\hat{x}_{t+1,t} = \Phi\hat{x}_{t,t}$
Predict Next Covariance Matrix	$Q_{t+1,t} = \Phi Q_{t,t}\Phi^T + V_y$

Chapter 3

Numerical Studies

The tools for state estimation of a PDE system have been presented in chapter 2. What has not been covered is how well state estimation using a Kalman filter and a Karhunen-Loéve-Galerkin model will work in practice. The reduced order model reduces the information complexity of the PDE system into a small tractable ODE system, a type of information compression. The proposed experiment to prove the state estimator works is estimating the concentration of a dye diffusing in gelatin. The experiment, however, may introduce unmodeled dynamics. A number of simulated experiments will be performed to verify the state estimator functions as expected, before applying the methodology to the experimental data. The simulated experiments are broken into three sections. First, the accuracy of the numerical solution to the diffusion equation is verified. Next, the performance of the reduced order model is confirmed. Third, the reduced order model is used to estimate state via the Kalman filter.

3.1 Numerical Solution to the Diffusion Equation

The numerical solution of the diffusion equation will be considered the true solution of the continuous problem. The accuracy of the numerical Method of Lines solver will be confirmed by comparing solutions using several different discretization mesh sizes and verifying the boundary conditions are satisfied. The numerical true solutions will be used with the Karhunen-Loéve expansion to find the empirical modes for reduced order model studies, state estimator performance studies and the physical experiment. Inaccuracies of the numerical solver will propagate to the reduced

order model and state estimator reducing accuracy. Solution results for the 1D and 2D diffusion equation are both verified.

3.1.1 Diffusion Equation in One Dimension

The one dimensional diffusion equation

$$\dot{u} = D\nabla^2 u$$

with diffusion coefficient $D = 1$, was simulated using an implementation of the Method of Lines solver with a first order second centered difference discretization in the spatial domain and the Matlab stiff ODE solver `ode15s`. The discretization of the spatial domain $\mathcal{D} \in [0\ 1]$ was performed with mesh sizes 0.01, 0.001, 0.0005. The initial condition and Neumann boundary conditions are given by

$$\text{IC} \qquad u(x, t = 0) = 1 \qquad x \in [0.3, 0.7]$$

$$\text{BC} \quad \tfrac{\partial u(0,t)}{\partial x} = \tfrac{\partial u(1,t)}{\partial x} = 0 \qquad t = [0, \infty)$$

Performance is evaluated by ensuring the boundary conditions are met. The solution to the homogeneous diffusion equation with homogeneous Neumann boundary conditions will maintain constant mass in the domain. The homogeneity of the diffusion equation means there are not source terms (actuators) in the domain to add or remove concentration. The homogeneous Neumann boundary conditions prevent any media from flowing in or out of the domain. Thus, integrating the concentration $u(x, t)$ over the domain at the initial time and final time should yield the same value. The initial conditions and final state values are integrated for each of the different discretizations. The initial conditions for the different mesh sizes have slightly different volume due to the discretization, making direct comparison of the volume less meaningful. The percent difference of the initial condition and final condition volumes are used to compare the error. Error values for mesh sizes 0.01, 0.001, 0.0005 are 2.33e-6%, 1.63e-4% and 6.96e-6%, respectively. The error of the three mesh sizes are of the same magnitude for fine and very fine discretizations affirming the 0.01 discretization is sufficently fine and the solver is performing as expected. The solution using the 0.01 discretization is accepted as being sufficiently accurate as a true solution for further numerical experiments. The solution is plotted for various time points in figure 3.1.

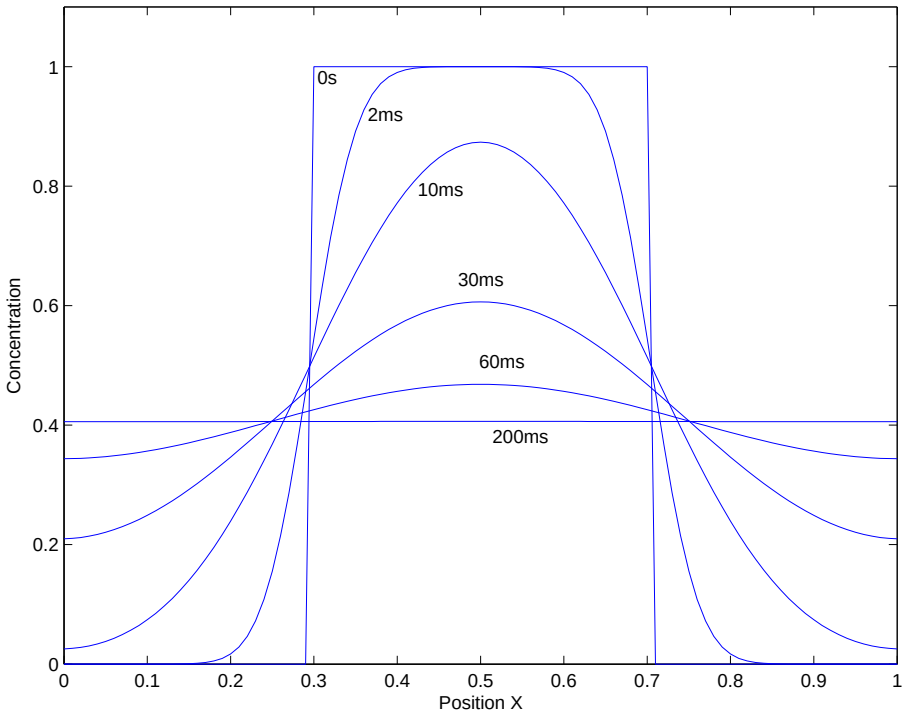

Figure 3.1: Solution to the 1D Diffusion Equation with Neumann BCs.

3.1.2 Diffusion Equation in Two Dimensions

Similar to the evaluation of the 1D diffusion equation the 2D diffusion equation will be evaluated by similar metrics. The homogeneous 2D diffusion equation is

$$\dot{u} = D\nabla^2 u$$

where the diffusion coefficent $D = 1$. The initial condition and boundary conditions are

$$\begin{array}{lcc} \text{IC} & u(x, y, t = 0) = 1 & x, y \in [0.3\ 0.7] \\ \text{BC} & \frac{\partial u(0,\ell_2,t)}{\partial x} = \frac{\partial u(1,\ell_2,t)}{\partial x} = \frac{\partial u(\ell_1,0,t)}{\partial x} = \frac{\partial u(\ell_1,0,t)}{\partial x} = 0 & x, y \in [0\ 1] \quad t = [0, \infty) \end{array}$$

The domain is discretized into a rectilinear domain in increments of 0.05, 0.02, 0.025 and 0.01 and simulated using the method of lines solver. As with the 1D case, the equation is homogeneous, and the boundary conditions are homogeneous, and thus there is no source term in the domain and the boundaries cannot have flow in or out of them. Integrating over the domain gives a mass which should be preserved through time. The percent difference of the initial and final volume are used to compare the different discretizations of the 2D diffusion equation.

3.2 Reduced-Order Model Performance

The state estimate is found using a Kalman filter and the reduced-order model as the dynamic model. An inaccurate model will lead to an inaccurate state estimate. The accuracy will be evaluated at several different orders of retained modes to verify the qualitative metric dictating retention of 99.9% of the system energy produces acceptable solutions. First, the empirical modes and associated eigenvalues/energy are shown. Second, simulation of the diffusion equation via the reduced-order model and comparison with the true solution will indicate performance. Third, the greater efficiency of the empirical basis is demonstrated by forming a reduced-order model using the analytical basis and then the empirical basis.

3.2.1 Karhunen-Loéve Decomposition

Displaying the mode shapes gives a visual interpretation of what dominant slow dynamics and fast high frequency dynamics comprise the system. Solutions for the 1D and 2D diffusion equations are decomposed to illustrate this.

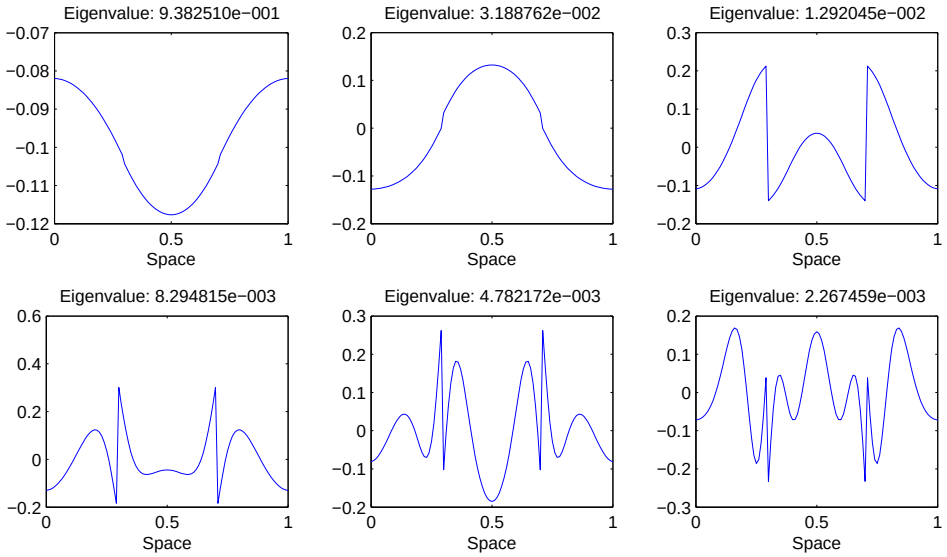

Figure 3.2: First six empirical orthogonal functions for 1D diffusion equation with Neumann BCs.

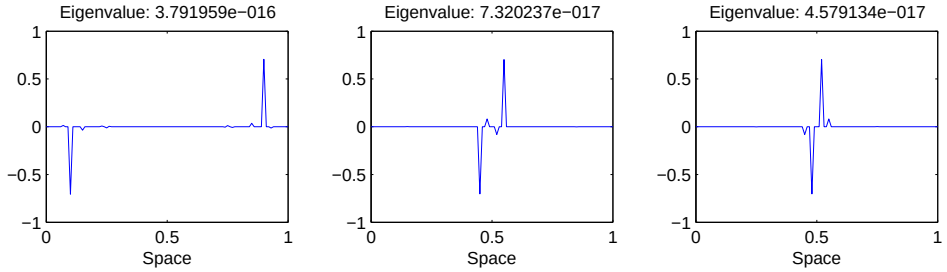

Figure 3.3: Last three empirical orthogonal functions for 1D diffusion equation with Neumann BCs.

The solution for the one dimension diffusion equation found in section 3.1.1 is used as the input ensemble to find the Karhunen-Loéve Decomposition. A full rank decomposition is performed. The first six empirical basis functions are found and displayed in figure 3.2. The associated normalized eigenvalue is reported at the top of each function figure. The last three empirical functions for the full rank decomposition are displayed in figure 3.3. The last three basis functions in figure 3.3 are nearly with zero eigenvalues meaning they do not contribute to the description of the system dynamics and will necessarily be discarded.

A decomposition of the results obtained in 3.1.2 is performed and plotted in figure 3.4. The associated normalized eigenvalue is indicated at the top of each figure.

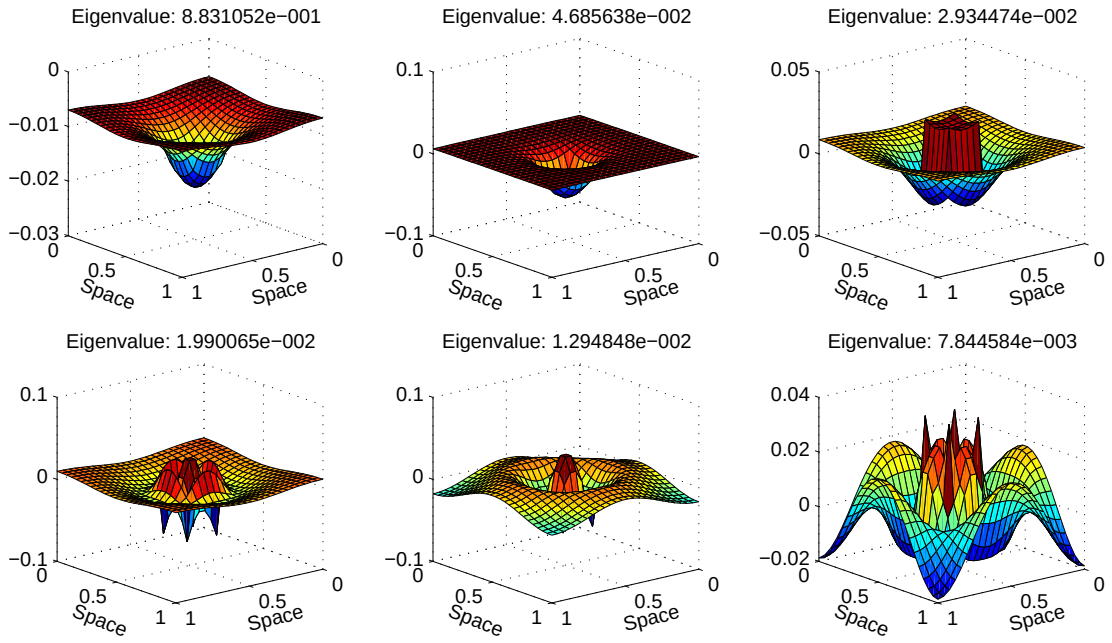

Figure 3.4: First six empirical orthogonal functions for 2D diffusion equation with Neumann BCs.

3.2.2 Reduced-Order Model Order Study

Accuracy of the reduced-order model is contingent on the number of modes retained, which has a direct impact on estimation accuracy. It is not known *a priori* what the error bound is for a reduced-order model formed from a certain number of basis functions. A qualitative metric asserts the system will be accurately described if 99.9% of the energy contained by the modes is retained. The analysis if performed for the diffusion equation in 1D with the assumption that the results similarly apply to the 2D case. The ability of the reduced-order model to approximate the original system is performed in two ways. First, the reduced-order model is simulated and the relative error through time is computed for models projected onto different numers of basis functions. Second, the maximum error between the true and approximated system for each order is used to form relating max error and basis size.

The relative error is defined as

$$e(t) = \frac{\|u(t) - \hat{u}(t)\|}{\|u(t)\|} \tag{3.1}$$

where the norm is the $\mathcal{L}^2$ norm for the Hilbert space $\mathcal{H}$. The true solution is $u(t)$ while the approx-

imate solution is $\hat{u}(t)$. The max error is defined as

$$e = \max_{t \in [0\ t_f]} e(t) \tag{3.2}$$

The 1D diffusion equation was simulated with the domain, initial condition and Neumann boundary conditions described in section 3.1.1. The simulation results were used as the input ensemble for the Karhunen-Loéve decomposition. ODE approximations for evolution dynamics of the first ten basis functions using the Galerkin method were found. Each of the ten reduced-order models were given the same initial condition and simulated for the same length of time as the original solution.

The qualitative energy metric used to determine the appropriate number of modes to accurately reproduce the system dynamics indicates the first three modes will produce a good model. It was expected that retention of modes greater than this number would produce better albeit small improvements. Performance of the reduced-order model of various orders is plotted in the top pane of figure 3.5. The relative error for the first six models are individually plotted in the lower half of figure 3.5. The 3^{rd} order model did produce a model with low error although the max error was approximately 15%. Retaining four modes reduces the max error to less than 5% and retaining more does not yield any significant improvements. The 3^{rd} order model will be used for the 1D numerical studes while a 4^{th} order model will be used for the 2D experiment to ensure low max error.

3.2.3 Fourier Basis & Empirical Basis Comparison

To further motivate using empirically determined basis functions over an analytic spectral basis Fourier analysis is used to generated a basis consisting of cosines to be used as the basis for the Galerkin Approximation. The cosines are found using the method described in section 2.2.2.

For the one dimensional case the first three empirical orthogonal functions are found using the Karhunen-Loéve Decomposition on the solution found in section 3.1.1. The ROM is then found using the linear Galerkin method. Comparison of the cosine basis solution, the empirical basis solution and the true solution are provided in figure 3.6. The figure clearly shows that the non-smooth initial condition is most accurately described by the empirical basis. As the solution advances temporally, the cosine basis solution improves, however, the maximum error is considerably smaller for the simulation with the empirical basis. The Karhunen-Loéve expansion is proven to produce an

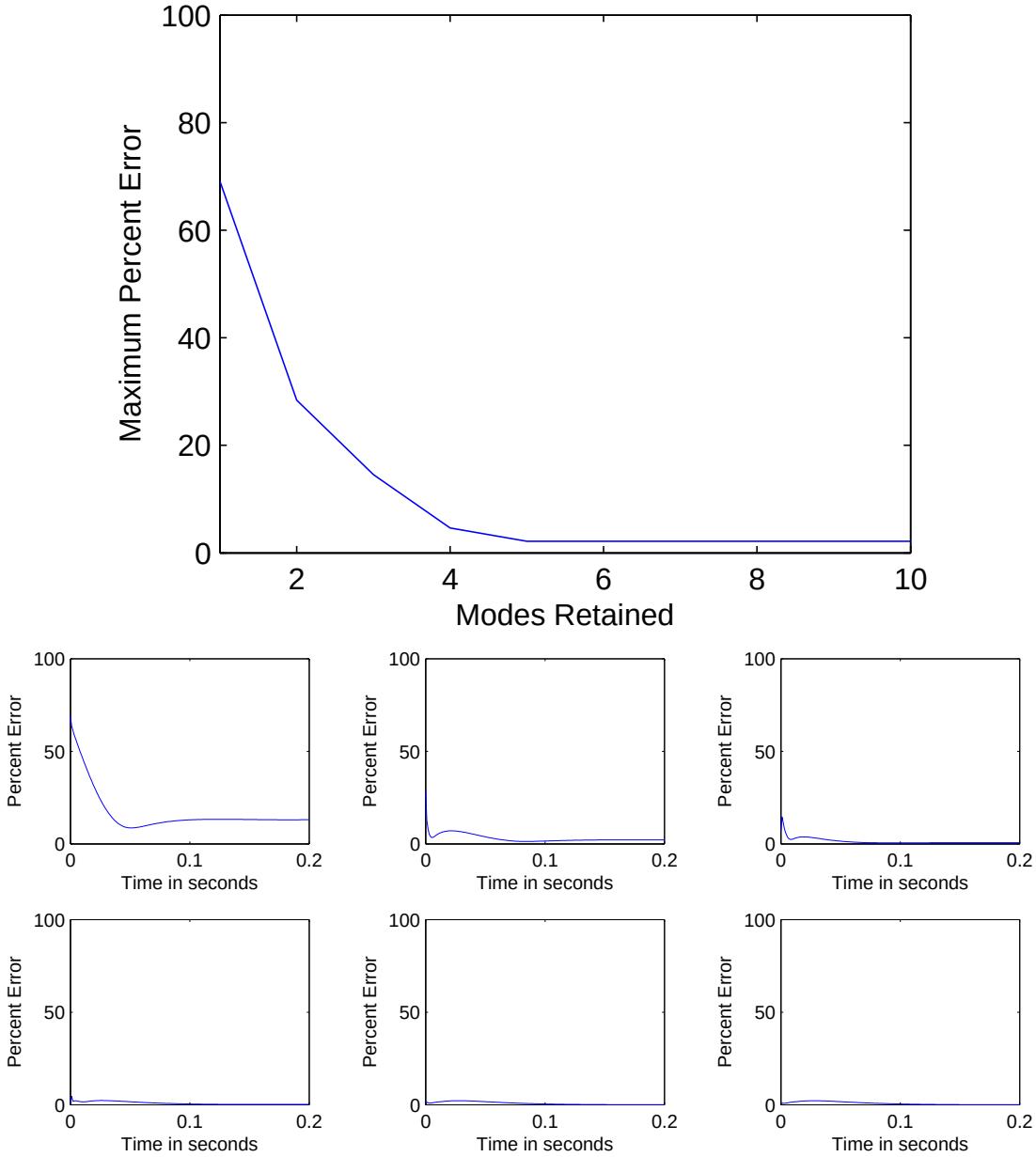

Figure 3.5: [Top]Maximum relative error for each reduced model order in one dimension. [Lower Six] Relative error profiles for first six order models.

optimal basis making this expected result.

To further underscore the advantage of the empirical basis, simulation of the two dimensional diffusion equation using a 16^{th} order Fourier basis as described in section 2.2.2 is compared with a 4^{th} order empirical basis. The empirical basis is formed by applying the Karhunen-Loéve decomposition to the results found in section 3.1.2. The solution error using the empirical basis is much smaller than the Fourier basis during the first 20ms. The solution obtained using the Fourier basis is particularly poor because the error is high, greater than 20%, while the interesting fast dynamics are occuring. Figures of the initial condition and solution at 10ms for the finite difference, Fourier-Galerkin and KL-Galerkin cases are in figure 3.7. The superior performance of the empirical basis was expected since the Karhunen-Loéve expansion is proven to be optimal.

3.3 Kalman Filter

The Kalman Filter is used to find an optimal estimate of state based on the available sensor measurements. The performance of the reduced-order model has been evaluated in section 3.2 indicating a 3^{rd} order model for the 1D diffusion equation and a 4^{th} order model for the 2D case will produce approximate solutions with low error (see section 3.2.2 for error rates). The estimator performance for the 1D diffusion equation using a 3^{rd} order approximate model and a high order finite difference approximation will be performed. The effects of varying sensors numbers for the estimator in 1D with no noise performed. Performance of the estimator is then evaluated for one and two dimensions. Finally the effects of sensor placement in the 2D domain is investigated.

3.3.1 Noiseless Filter Performance

Estimator performance is first evaluated using a reduced-order model and a high dimensional finite difference approximation to affirm the estimator is working well. Due to storage requirements and lengthy computation times for accurate explicit Euler solutions, the comparison will only be made in the one dimensional case, leaving the results to motivate that the 2D case will behave well.

Performance is assessed in the absence of sensor and process noise. The 1D diffusion equation was simulated using a method of lines solver as described in section 3.1.1. A 3^{rd} order model is obtained using the Karhunen-Loéve-Galerkin approach. The state is estimated using Kalman filters formulations found in sections 2.5.3 and 2.5.4. The time steps for the KLG estimate are 1ms while

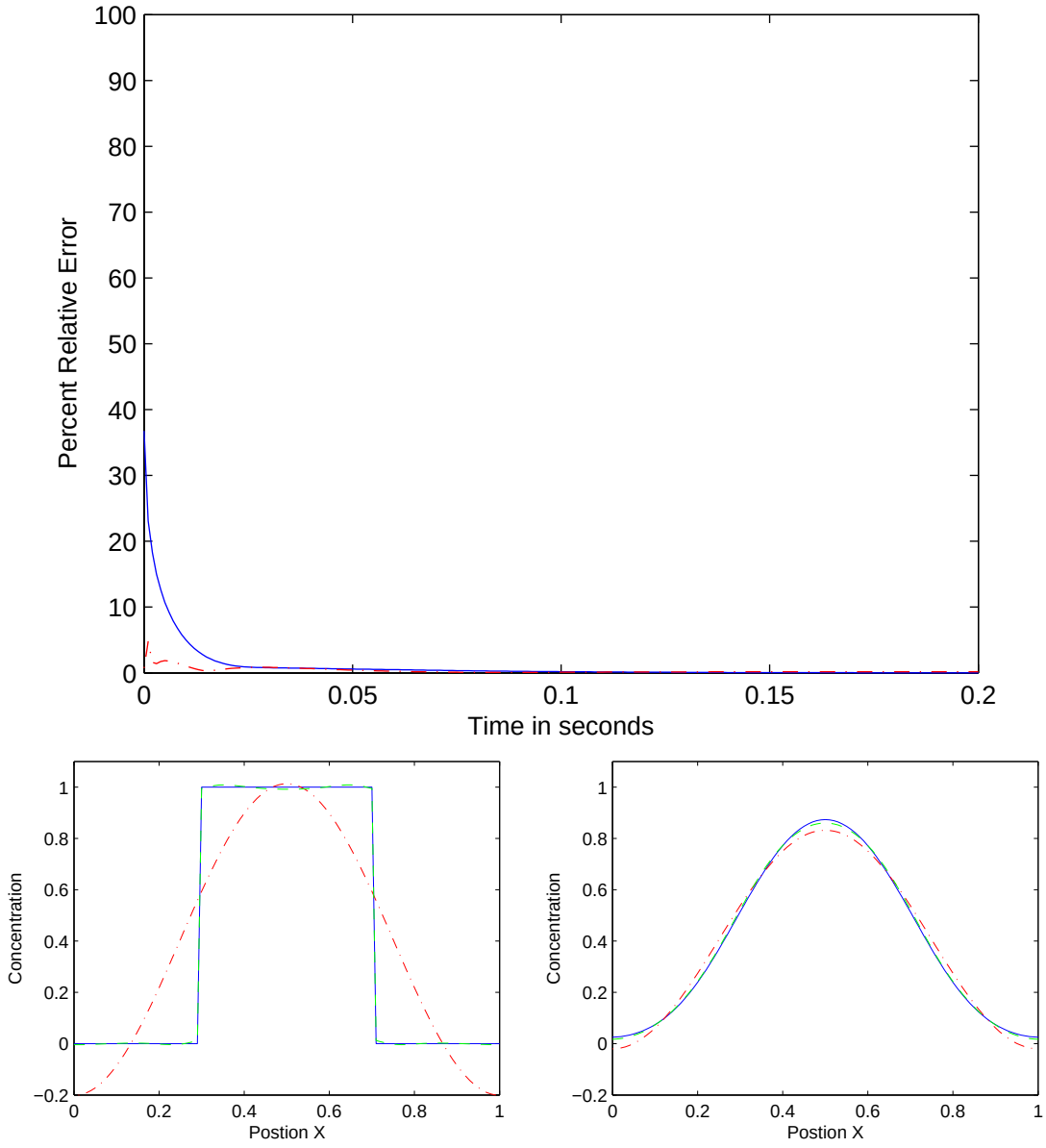

Figure 3.6: [Top] Empirical (dashed red) and Fourier (solid blue) basis relative error for 1D diffusion equation. [Bottom] Solution snapshots at 0s (left) and 10ms (right) for finite difference solution (solid blue), 3^{rd} order Fourier-Galerkin (dot-dash red) and 3^{rd} order Karhunen-Loéve-Galerkin (dashed green).

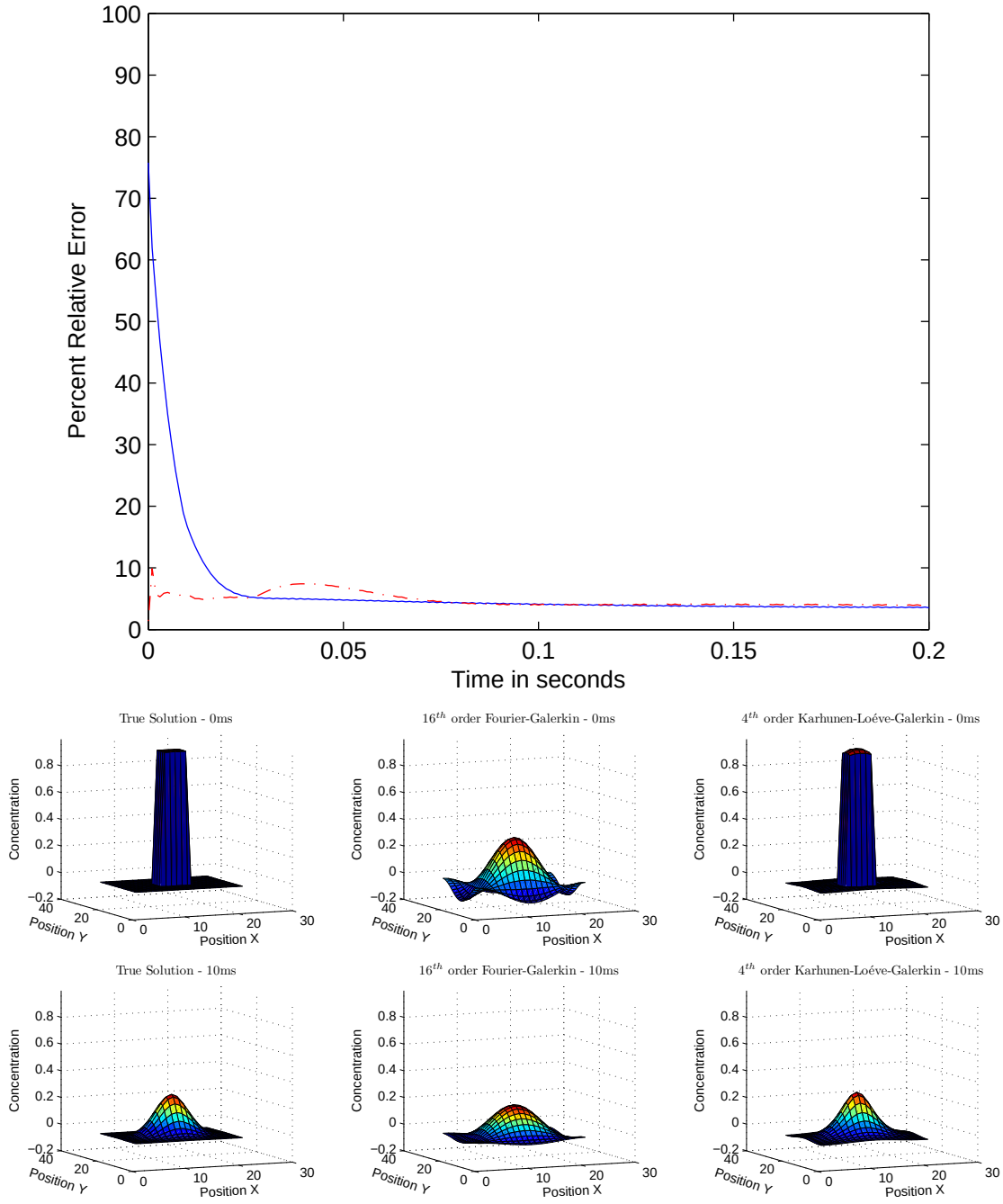

Figure 3.7: [Top] Empirical (dashed red) and Fourier (solid blue) basis relative error for 2D diffusion equation. [Middle] Solution snapshots at 0s for finite difference solution (left), 16^{th} order Fourier-Galerkin (middle) and 4^{th} order Karhunen-Loéve-Galerkin. [Bottom] Solution snapshots at 10ms, same ordering as Middle.

the explicit Euler estimator uses a $25\mu s$ time step to enforce the Courant-Friedrichs-Lewys stability requirements. Eleven noiseless measurement sensors are placed evenly in the domain. Solution cross-sections of reduced-order model and explicit Euler implementations are shown in figure 3.9 and 3.10 respectively. The state evolutions are displayed in 3.8. The state trajectories at the sensor locations are shown for the actual (blue circle) and estimated state (red dot). The relative error for each solution is plotted in figure 3.3.1. The explicit Euler estimator provides superior performance save for the very first time step with nearly 0% estimation error. The reduced-order model produces more error than the finite difference approximation but the relative error evolution is very simlar to what is displayed in the 3^{rd} order simulation in 3.2.2, both of these seek to approximate the same true solution. The similarity in the estimator performance and the reduced-order model simulation indicate the estimator is operating near the error limit of the reduced-order model.

3.3.2 Noisy Filter Performance - 1D

The configuration described in section 3.3.1 is reproduced. The sensor measurements are corrupted with zero mean white Gaussian noise with a standard deviation of 0.1. The state trajectory of the system estimate is plotted in figure 3.13 and cross-sections of the state estimate are plotted in 3.12. The error evolution for the system is plotted in 3.14, the estimate error is less than 5% after 5ms. Figure 3.15 depicts the difference of the true solution and the estimate, the estimate is smooth in space noisy in time.

3.3.3 Noisy Filter Performance - 2D

The diffusion equation is simulated as described in section 3.1.2 and corrupted with additive zero mean white Gaussian noise to serve as sensor measurements. A 3^{rd} order reduced-order model is constructed using the noiseless result of section 3.1.2. Nine sensors are placed in the domain, figure 3.18 middle depicts the placement and the error evolution. Comparison snapshots of the system at various time points for true, noisy and estimated state are shown in figure 3.16. A nondimensional temporal cross-section of the state estimates is give in figure 3.17. The error estimate for the 2D filter does not get driven down as fast as the 1D filter. The estimator takes over 30ms to get the estimate below 20% error. The sensor placement and number will be examined in light of the poor performance.

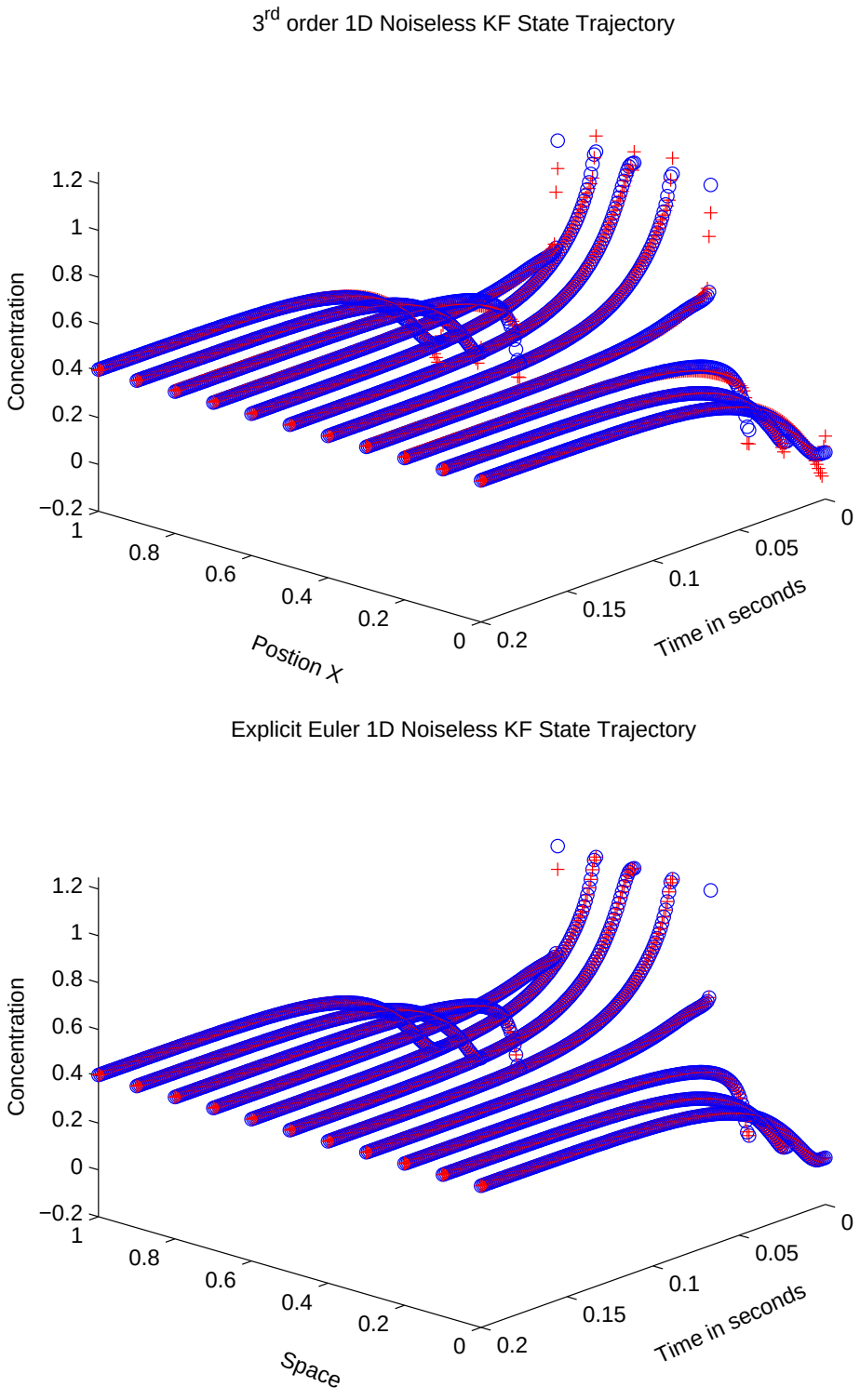

Figure 3.8: [Top] Reduced-order model Kalman filter state trajectory for true (blue circle) and estimated (red +) state [Bottom] Explicit Euler Kalman filter state tracjectory

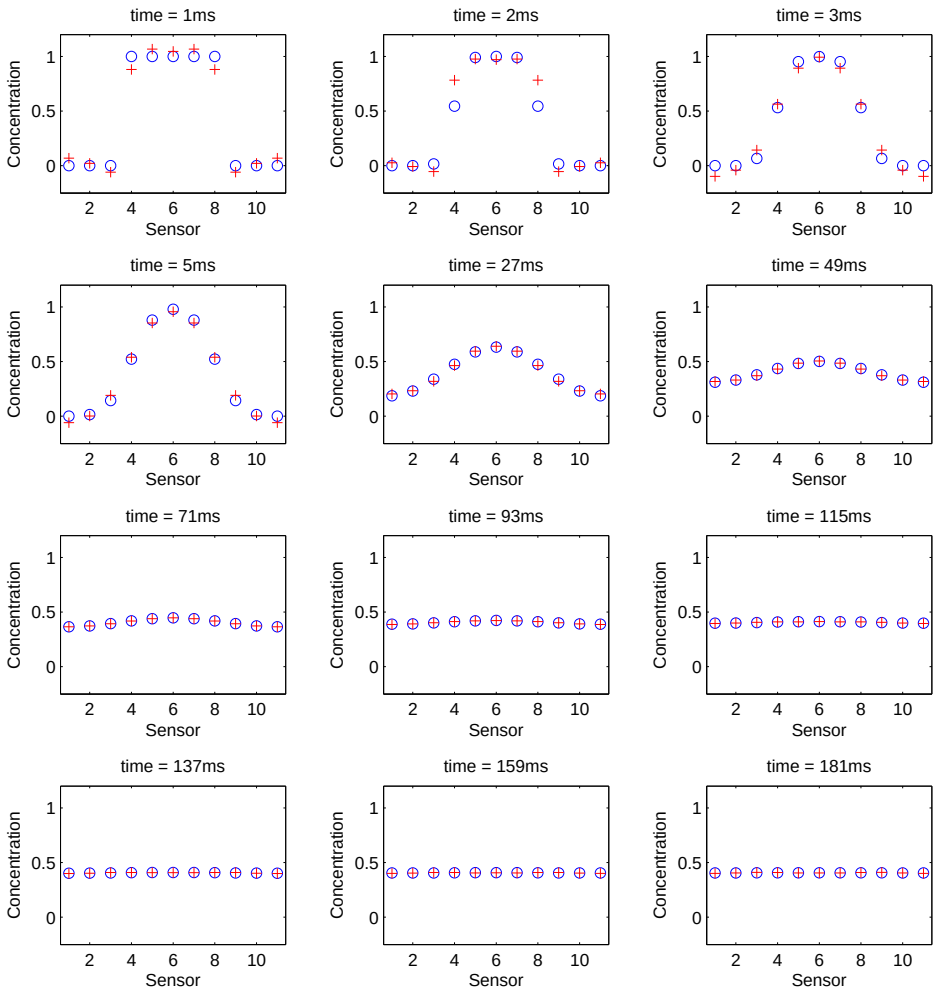

Figure 3.9: Reduced order model Kalman filter state temporal cross-sections for true (blue circle) and estimated (red +) state shown in twelve small multiples. Each horizontal axis corresponds to a noiseless measurement sensor; each vertical axis denotes concentration.

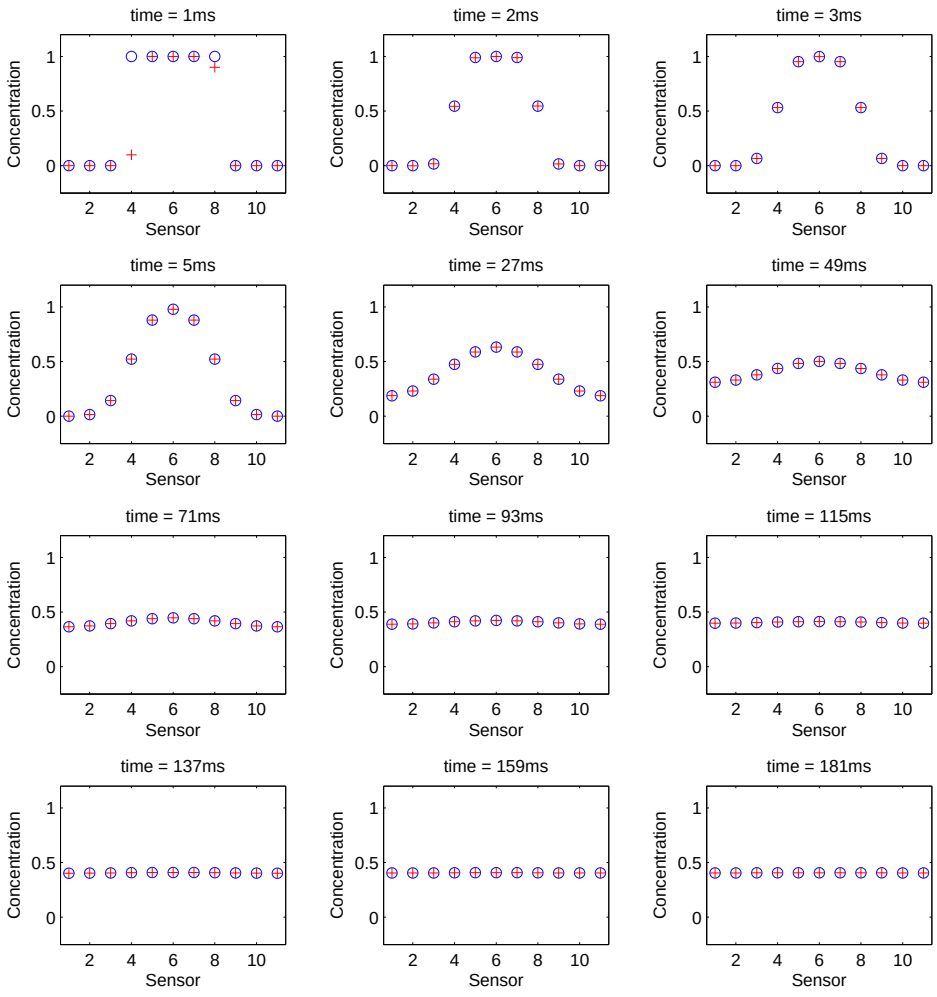

Figure 3.10: [Top] Explicit Euler Kalman filter state temporal cross-sections for true (blue circle) and estimated state (red +) shown in twelve small multiples. Each horizontal axis corresponds to a noiseless measurement sensor; each vertical axis denotes concentration.

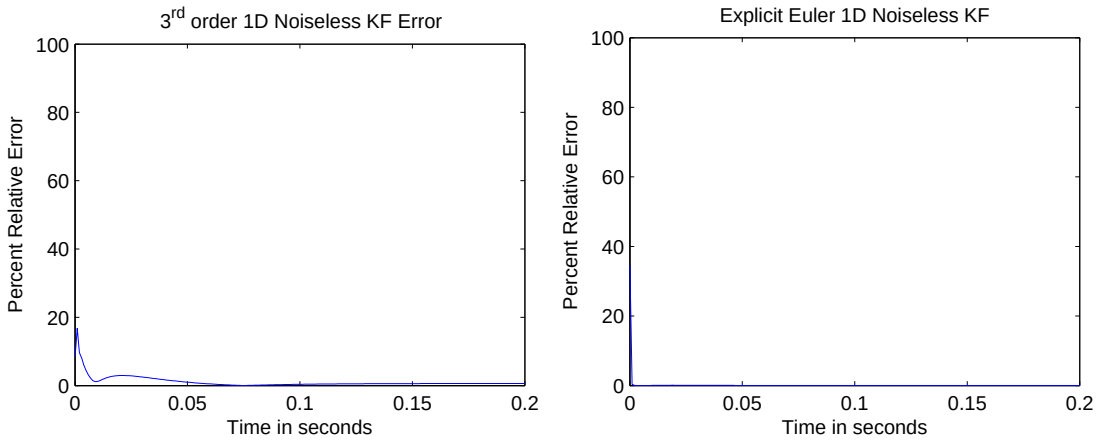

Figure 3.11: [Left] Error evolution for state estimate using a 3^{rd} order approximate model. [Right] Explicit Euler state estimate error

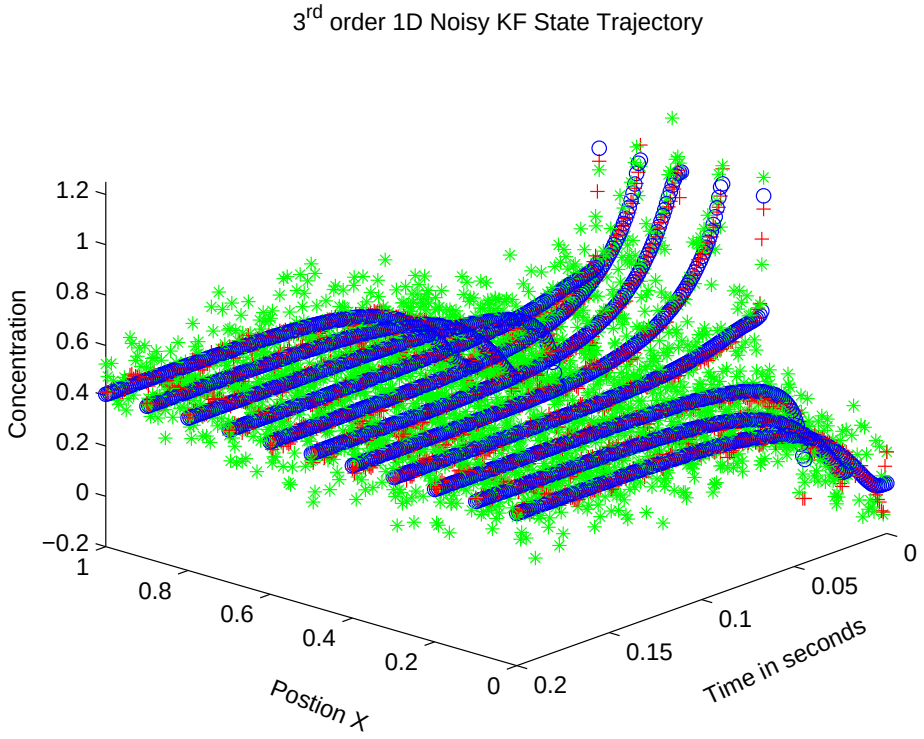

Figure 3.12: Noisy reduced-order model Kalman filter in 1D sensor state trajectory. true (blue circle) estimate (red +) and noisy measurement (green asterisk)

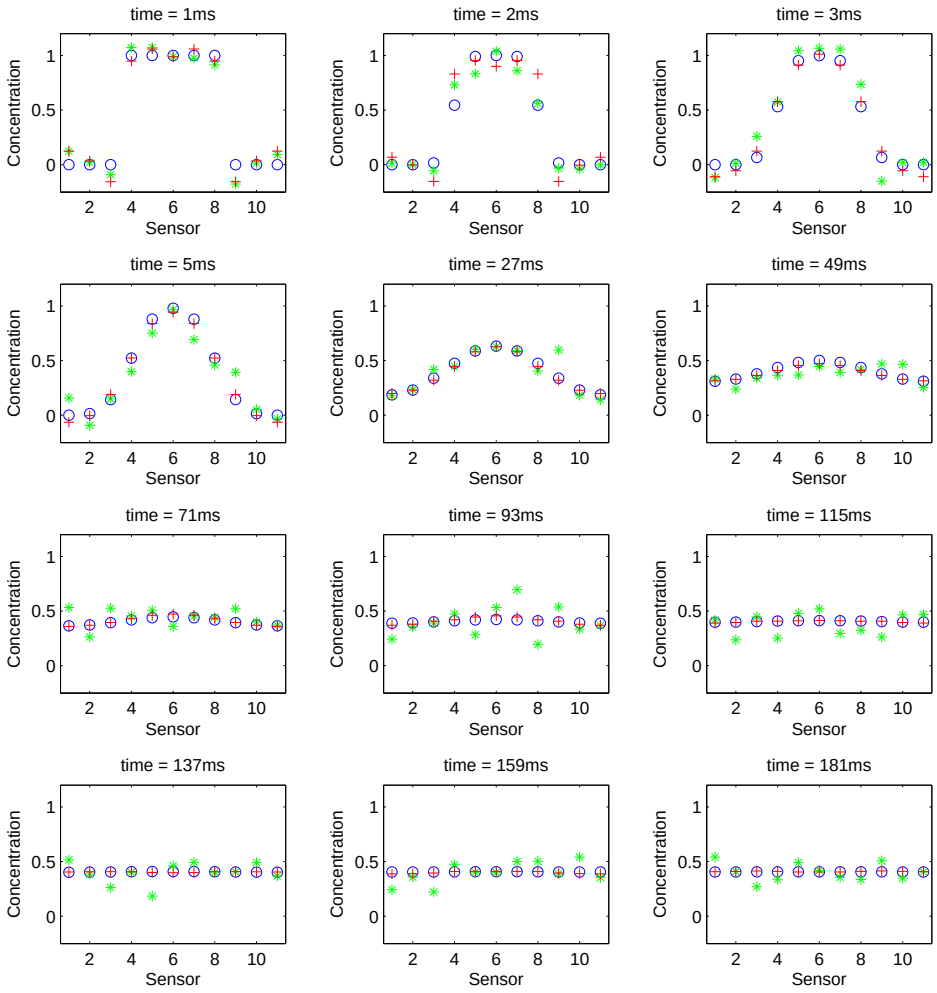

Figure 3.13: Temporal cross-sections of noisy reduced-order model Kalman filter in 1D shown in lower twelve small multiples. Each horizontal axis corresponds to a noisy measurement sensor; each vertical axis denotes concentration. State legend: true (blue circle) estimate (red +) and noisy measurement (green asterisk)

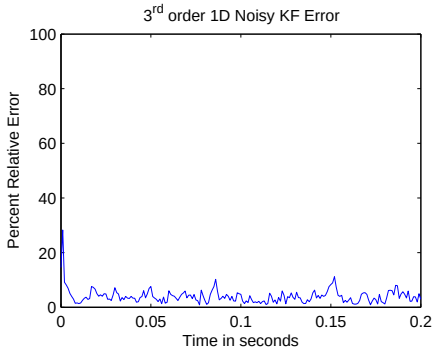

Figure 3.14: Error evolution for 1D Kalman Filter with Neumann boundary conditions

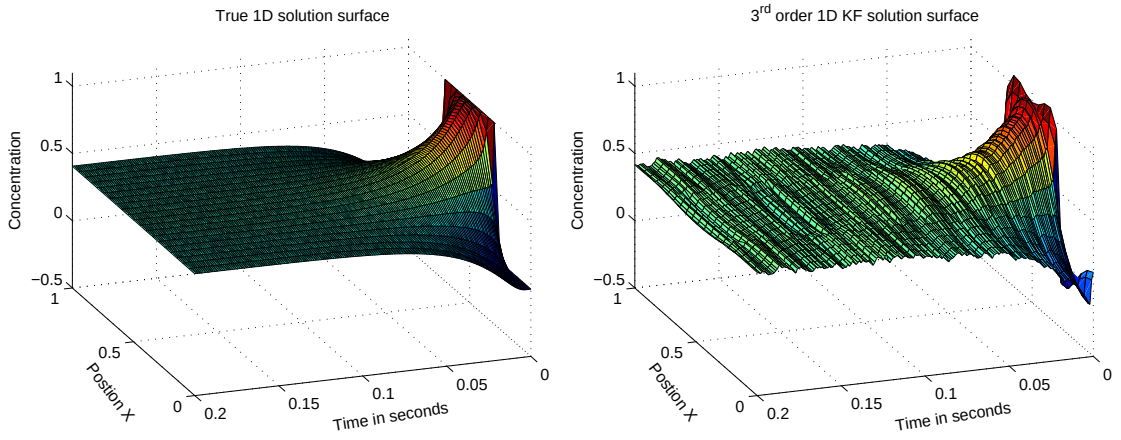

Figure 3.15: [Left] Error evolution for state estimate using a 3^{rd} order approximate model. [Right] Explicit Euler state estimate error

3.3.4 Noisy Sensor Study

The effect of sensor placement and number are investigated for the 2D system. The simulation experiment results from section 3.3.3 motivate this. The noisy sensor study conducted in this section is meant to examine the effect of sensor placement and number empirically to create an intuition to be used with the physical experiment.

Sensors were placed at various locations and relative error measurements taken for no measurement error and additive zero mean white Gaussian noise with 0.05 standard deviation. Sensor location plots and relative error measurements are plotted in figure 3.18. Problems estimating the state in the presence of noise are elucidated. The 16 sensor case becomes ineffective in the presence of noisy. By ineffective what is meant is error rate is approximately 10% while the interesting system dynamics are ocurring. Placing a sensor where the initial concentration is known to be *a priori* solves the problem.

3.3.5 Summary

The tools developed in chapter 2 were implemented in a numerical computing environment and confirmed to work. A numerical solution to the 1D and 2D diffusion equation were shown to be accurate and accepted as the solution to the continuous problem. A reduced-order model was constructed from a Karhunen-Loéve decomposition of numerical simulations for the 1D and 2D diffusion equation. The reduced-order model was shown to reproduce system dynamics with a 3 or

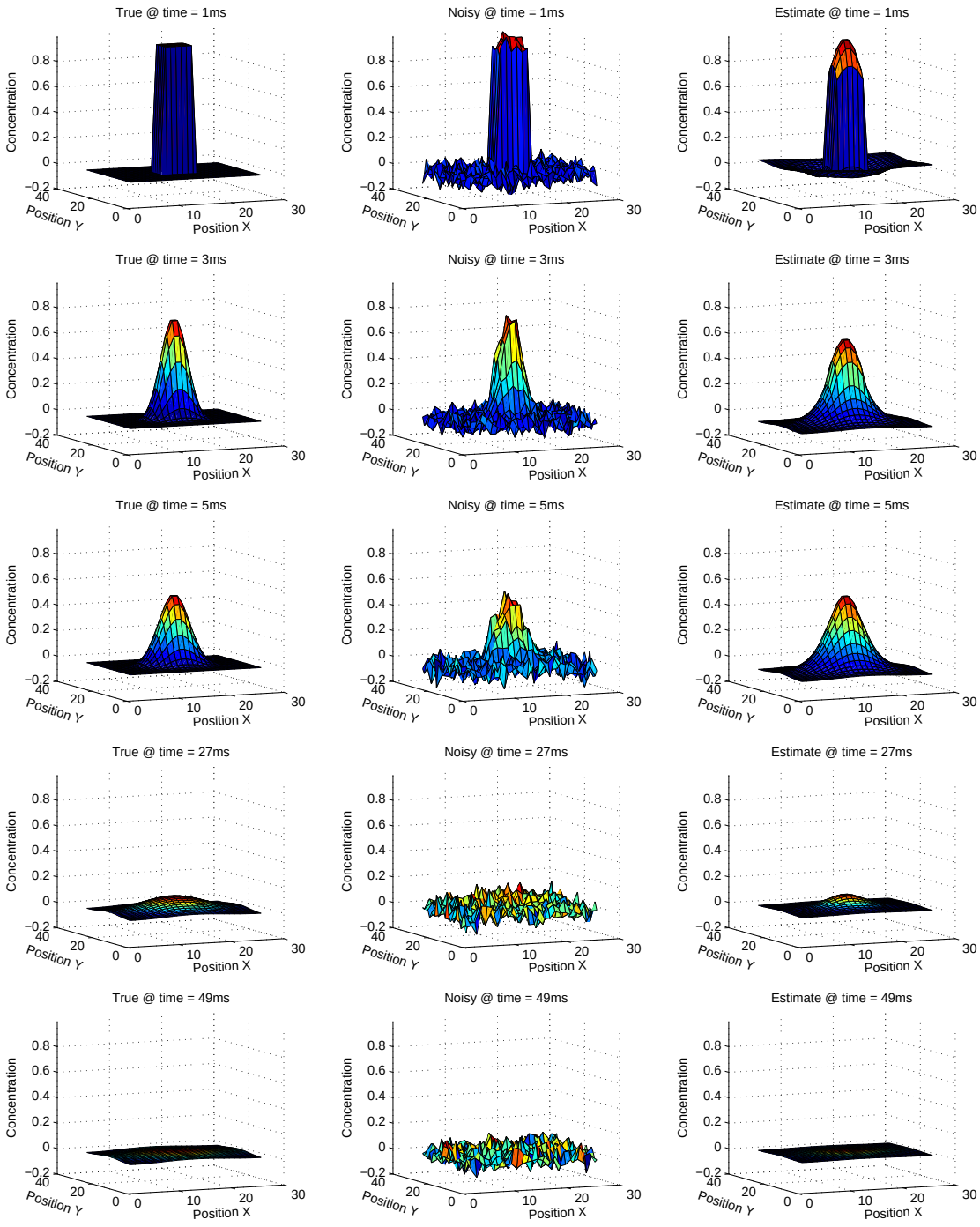

Figure 3.16: True, noisy and estimated states for 2D Kalman filter at various time points

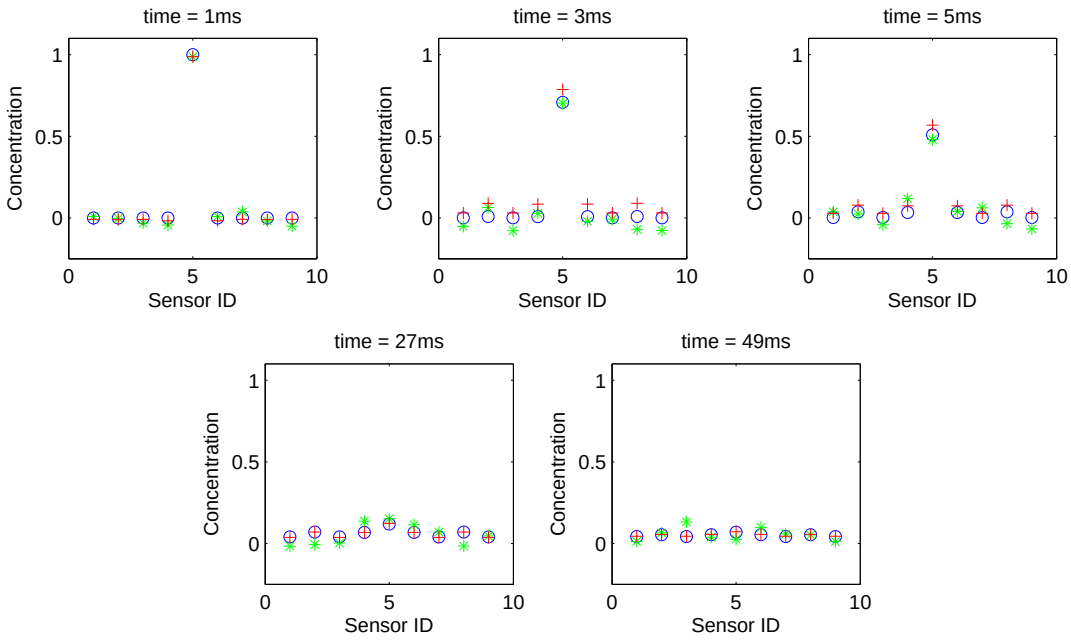

Figure 3.17: Non dimensional state trajectory cross-section.

4 ODE approximation. The advantage of using an empirical basis was demonstrated by comparison with a cosine basis, the cosine basis cannot reproduce the dynamics well unless many basis functions are used. The reduced-order model Kalman state estimator was shown to produce error near the limit of the reduced-order model for no noise and 11 sensors. Effects of sensor placement and number on the error of the estimate was investigated for the 1D and 2D diffusion equation for the noisy and noiseless case. Placement and number of sensors required were not determined analytically.

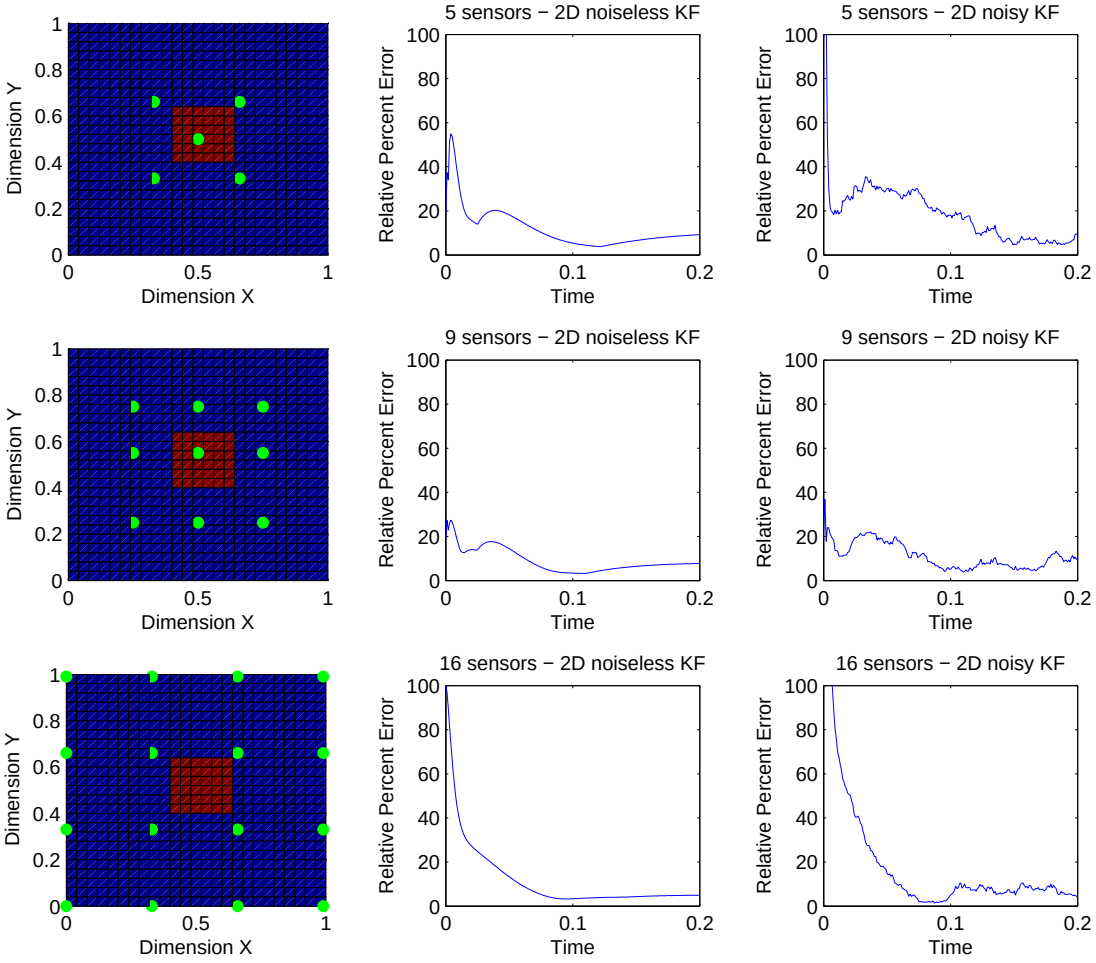

Figure 3.18: Sensor, Noisless, Noisy Error plots for 5, 9 and 16 sensors

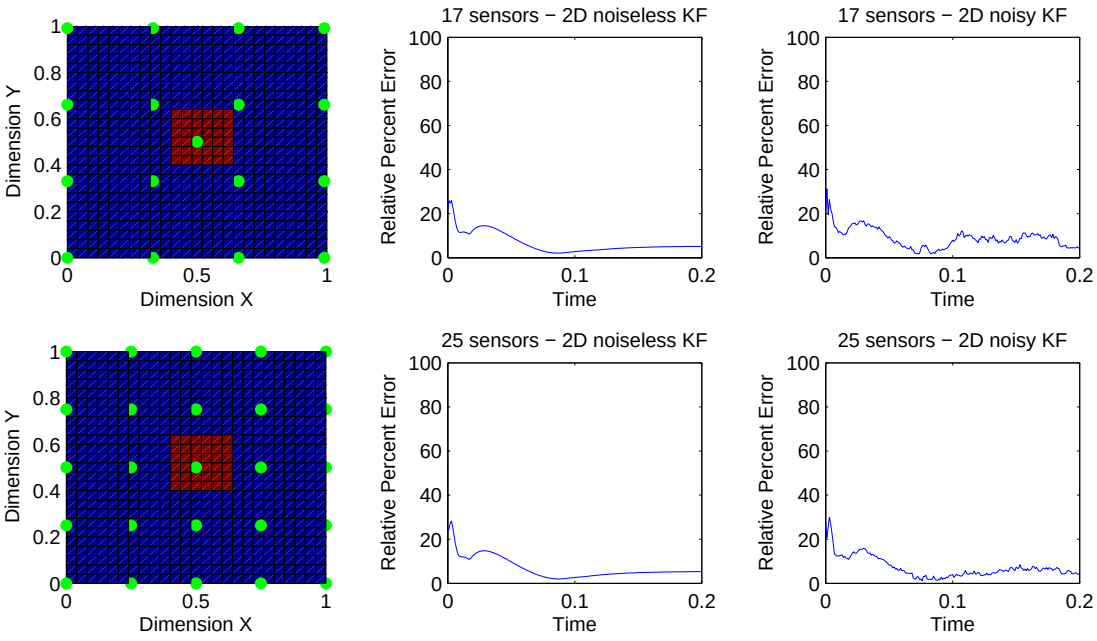

Figure 3.19: Sensor, Noisless, Noisy Error plots for 17 and 25 sensors

Chapter 4

Experiment

The objective of this thesis is to estimate the state of a diffusion process in a biologically relevant material. The mathematical tools to reduce the diffusion equation into a small set of ODEs have been presented. The methods examined in the Numerical Studies and confirmed to function will now be implemented in a physical experiment. As established in the introduction, the process of oxygen diffusion through tissues and collagen is important to many biological processes. The medium that will serve as the biologically relevant material is gelatin. A drop of dye will be injected into the gelatin and observed using a camera. Only a few pixels, i.e. sensors, will be used to estimate the state, but the entire image will be available to evaluate the estimator performance. The estimate of dye concentration will serve as a proof of concept of the application of these estimation problems to biological systems. The experimental apparatus developed here will provide a testbed for further work in state estimation.

4.1 Experiment Platform

A general test platform has been developed which permits experimentation with biologically relevant samples. The platform will be able to accommodate samples of of varying size and boundary conditions. A 60mm×60mm lighting surface will accommodate either a small 13mm×13mm sample holder to enforce homogeneous Neumann boundary conditions or a larger sample holder approximating homogeneous Dirichlet boundary conditions. The sample is back lit via a Dolan-Jenner DC950 fiber optic light source which is diffused through frosted acrylic producing a uniformly lit

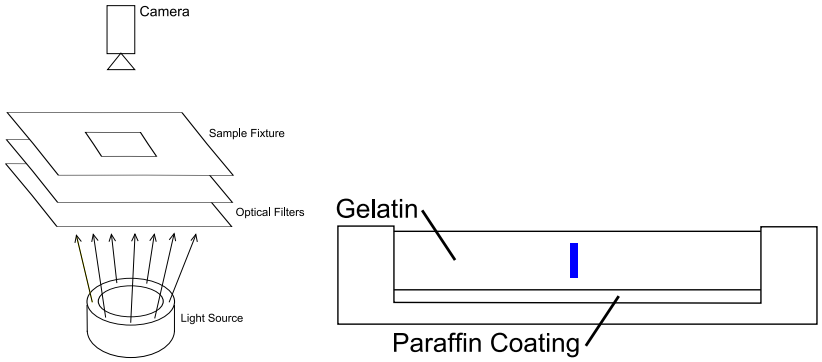

Figure 4.1: [Left] A schematic of the test platform. A light source is diffused through filters producing a uniformly back lit fixture to hold the sample during observation. [Right] Cross section depicting the hydrophobic paraffin coating, gelatin and ideal ink injection in a sample tray.

surface. Sample trays are manufactured to contain gelatin and also to define boundary conditions. An acrylic hood is placed over the sample to slow dehydration of the gelatin. A variable size mask is placed on the the fixture, allowing a sample tray to be affixed with repeatable precision. Data is collected using a Lumenera Infinity microscope camera. The data is subsequently analyzed in a numerical computing environment.

4.2 Sample Preparation

Knox® brand flavorless gelatin is used as the hydrogel medium in which diffusion will be studied. The manufacturer's suggested gelatin mixing ratio is one packet gelatin mix to one cup boiling water. The content of a single gelatin packet was found to be on average 7.1 grams. The quantity of gelatin mix is reduced producing a gelatin which exhibits the diffusion process quickly while ensuring no flow of ink is allowed. Ingredient ratios of water to gelatin were tested to qualitatively determine the optimal gelatin stiffness. McCormick® blue pigment at full concentration was used. Ratios 1:1, 1:4, 1:8, 1:10 of gelatin to water were tested. The original ratio 1:1 required several days to diffuse. Ratios 1:8 and 1:10 exhibited non-uniformity in the diffusion of dye. The 1:4 ratio demonstrated the diffusion process in a timely manner while maintaining a predictable diffusion process. Samples are prepared using the 1:4 mixing ratio of water to gelatin. The sample storage fixture provides reduces dehydration of the collagen incurred by the low humidity environment found in a refrigerator. A water reservoir is placed in an enclosed container and each sample covered.

McCormick® blue food dye (water, propylene glycol, FD&C Blue 1, 0.1% propylparaben) is

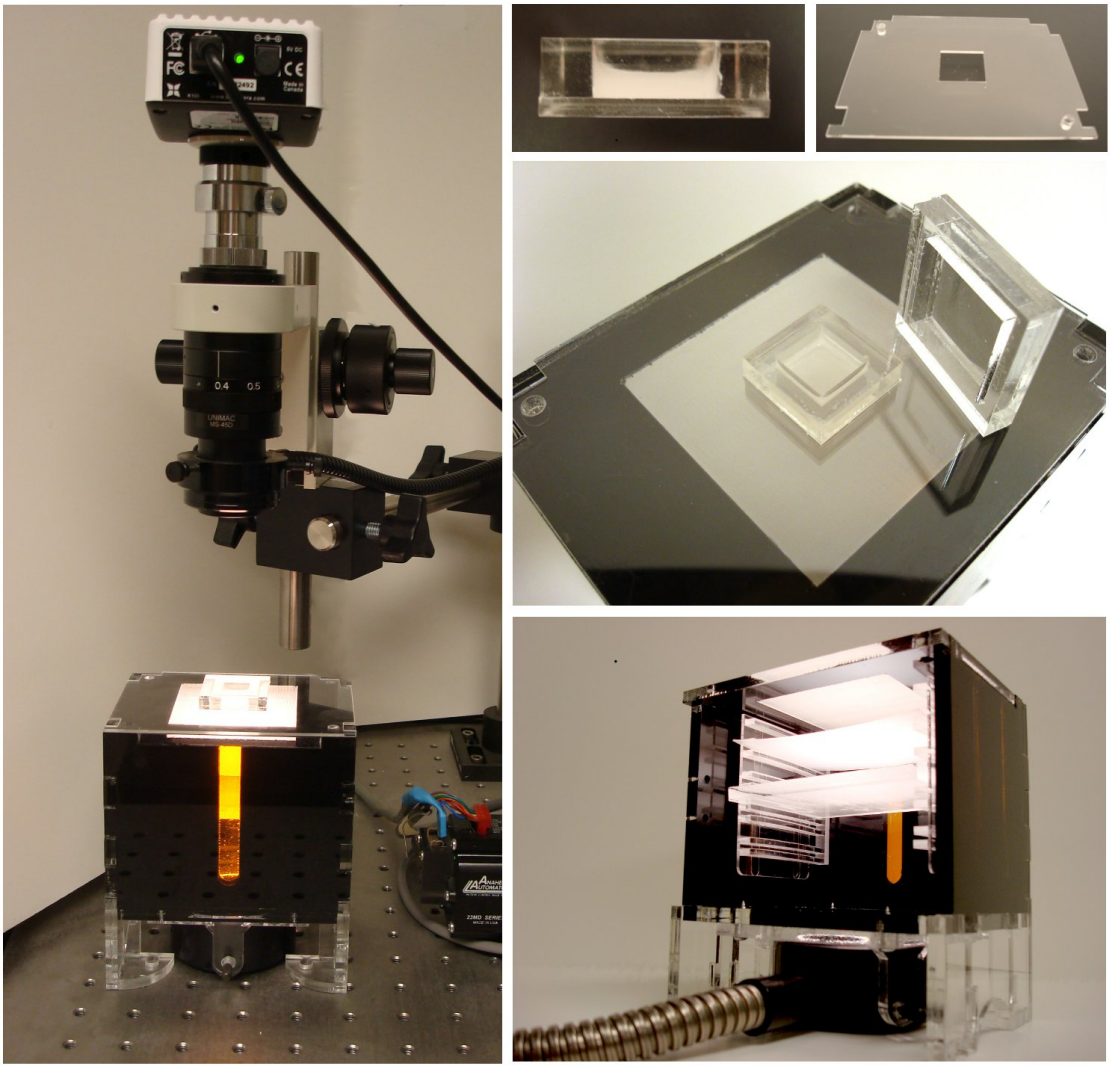

Figure 4.2: [Left] Diffusion test system and microstope. [Top Left] Side view of sample holder depicting paraffin coating. [Top Right] Replaceable fixture mask. [Middle] Sample holder placed in fixture mask on lighting surface. Moisture barrier standing on edge. [Right Bottom] Rear service panel removed revealing optical filters.

used as the pigment source. Trials of diffusion of several different dye concentrations were conducted to evaluate use of a camera as a concentration sensor. At high concentrations all light is blocked by the dye, once all light is blocked increasing the dye concentration further is not sensed by the camera. At high concentrations of dye act as a source term in the diffusion process. If the diffusion process is homogeneous with homogeneous Neumann boundary conditions, then the volume at the initial time and final time will be equal, this can be found by summing the pixel values of the image. For aqueous dye solutions above 20% the initial and final volumes differed by one to two orders of magnitude. It was found that a 1.25% aqueous soulution of blue dye differs by a factor of 1.5 to 2. The 1.25% solution was chosen since it shows interesting dynamics of the system while nearly satisfiying the ideal case.

Preliminary tests of the diffusion platform revealed a problem with pigment injection into the sample space. Injection of the pigment near the bottom of the gelatin causes pigment to flow along the bottom surface of the sample holder thus obscuring the diffusion dynamics with an unmodeled flow term. Paraffin is used to create a hydrophobic coating on the sample holder bottom to discourage flow.

4.3 Data Processing

Data is captured at regular intervals using the Lumenera Infinity camera. A background image of the sample holder with no injected pigment is captured. Images are converted from RGB to grayscale. Ideal concentration profile is highest concentration corresponding to gray value 255 while no concentration corresponds to 0. The inverse is obtained while collecting data; the system snapshot at each time increment is subtracted from the background producing the expected profile and removing static structures in the image. The image is cropped to include only the region of interest and resized into two data sets of 21 and 101 pixels square. Figure 4.3 illustrates the process.

The diffusion coefficient of the acqueous solution of dye in gelatin is not known outright. The diffusion coefficient is fit to the experiment snapshots using a gradient descent approach. The first snapshot from the experimental data is used as the initial condition for the 2D diffusion equation and simulated with a coarse 21 element discretization on each axis. The algorithm runs simulations for differing diffusion coefficients until the integral of the relative error is minimized. The diffusion equation is then simulated at a fine 101 element discretization on each axis. The simulation result

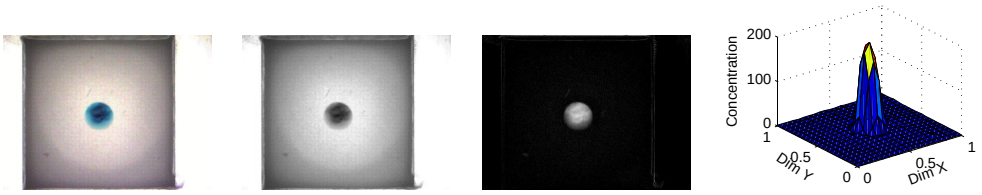

Figure 4.3: RGB original, grayscale, foreground subtracted image, cropped image

is decomposed using the Karhunen-Loéve expansion and a reduced-order model found using a linear Galerkin method. The reduced-order model is then used in a Kalman filter to estimate the state of the system snapshots using only a small number of pixels in the image as sensors.

4.4 Results and Discussion

The diffusion process of 1.25% acqueous solution of blue dye in 1:4 gelatin is captured at 15 second intervals for 125 minutes. The data is processed as described in section 4.3. The processed system states are then used to fit a diffusion coefficient to the empirical data. The relative error of the best fit 2D homogeneous Neumann diffusion equation is plotted in figure 4.4. The absolute difference of the true and estimated state is displayed in 4.5. Watching the evolution of the physical system and the numerical simulation side by side it is obvious a problem lies in the experiment data. The numerical simulation is forced to be homogeneous with homogeneous Neumann boundary conditions, therefore it is known the numerical simulation has no source term or ability to accrue mass as the time advances. The physical system is homogenous with homogenous Neumann boundary conditions since the only addition of mass (dye) is at the initial condition with no dye added at a later time. Also, the volume is finite so the mass may not flow out, therefore the total mass in the physical system should not change. As the state for the physical system evolves, pixel values indicating mass concentration at the initial condition do not change much while the values of the neighoring area increase. Both the numerical simulation and the physical system should maintain the same amount of mass for all time. As the total mass in the physical experiment seems to increase the numerical model maintins causing the solutions to diverge as time advances. Although the dye was diluted, the camera remains slightly inaccurate for sensing concentration. Another effect which artifically increases the concentration is formation of a bubble in the gelatin after the dye is injected. The results of the experiment do not reflect this, however, it was noted in several trials. The walls of the

bubble obscure light which appears as a high concentration to the camera. When this bubble pops it appears as a sudden decrease in concentration.

The diffusion model fit using the gradient descent approach is simulated for the same time period as the physical experiment. The empirically fit diffusion coefficient was found to be $D = 3.267e-7$. The simulation results are then decomposed into empirical modes using the Karhunen-Loéve expansion. A 4^{th} order approximate model is then found using the Galerkin projection. The state estimator is then evaluated using the experiment data. A small number of observation points are taken from the series of pictures by sampling only a few pixels. The pixel values are then used by the reduced-order model Kalman filter to estimate the state. The sensor locations and error for the state estimator are depicted in 4.8. Comparisons of the camera observations and the state estimator are available in figures 4.6 and 4.7 at regular time intervals. The performance of the state estimator was much better than the reduced-order model. The reduced-order model maintains greater than 30% error for most of the time period while the state estimator drives the error to approximately 15% for the most of the experiment.

The steady state error observed in the state estimator for real data is 10% higher than that estimated for noisy simulation data. One reason for the high error rate is inhomogeneity in the experiment data. The camera senses high concentrations as low light levels. Even at low concentrations of dye the camera still observed an appararent source term. As the dye diffused outward the camera perstistly detected the same dye concentration at the intial condition although the true concentration was decreasing. Inhomogeneous behavior causes two problems. First, the diffusion coefficient is not known directly; simulations of the diffusion equation are run with several different diffusion coefficients to determine the best fit coefficient. Simulating an inhomogenous system with a homogenous model will not produce an exact solution. Secondly, the model which is formed using the Galerkin projection is composed of empirical orthogonal functions which are recovered from simulation of an homogenous model. The Karhunen-Loéve-Galerkin reduced-order model can not reproduce dynamic behavior it has not seen before such as inhomogenous behavior if a homogenous input ensemble is used. Accurately determining the diffusion coefficent using a standalone experiment would allow a more accurate input ensemble but would not resolve the sensor problem. Improvement in concentration estimation could be made by characterizing the camera allowing more accurate observations to be made. Relative error of a least squares fit of the full camera data to the empirical functions at each time step is displayed in figure 4.4. The solution

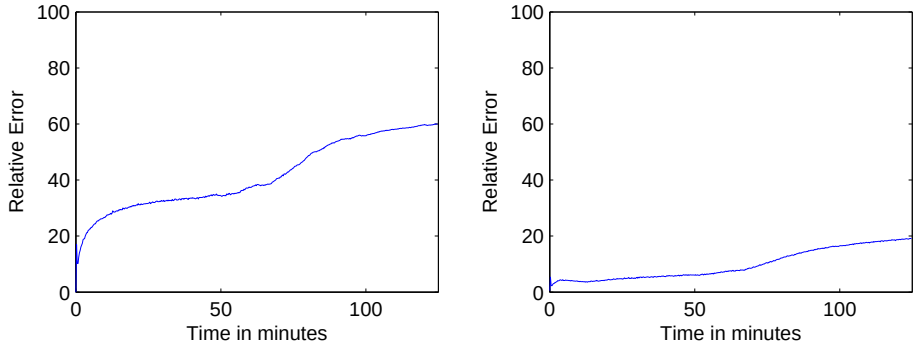

Figure 4.4: [Left] Relative error for numerical model using empirical diffusion coefficient. [Right] Least squares fit of full camera data to basis functions at each time step.

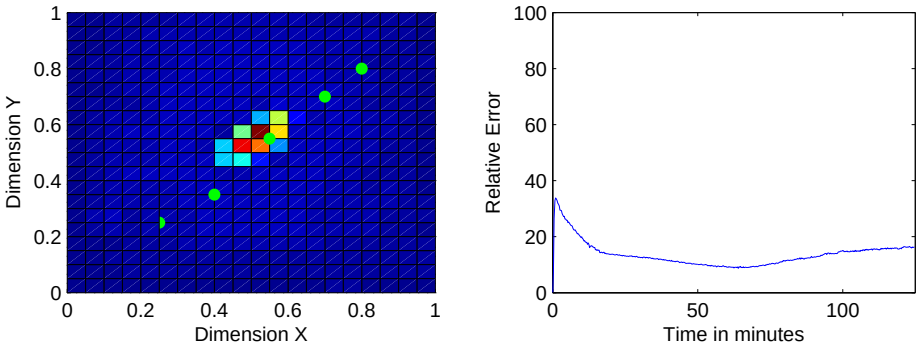

Figure 4.5: [Left] Sensor locations overlaid on aerial view of initial condition. [Right] Error evolution of Kalman filter

gradually diverges as time advances due to the inhomogeneous behavior. The higher error of the state estimator for the first 70 minutes is most likely due to to an overestimate of the noise on the sensor data. This causes the estimator to place more trust in the current state estimate which in turn causes the estimate to slowly converge to the true state.

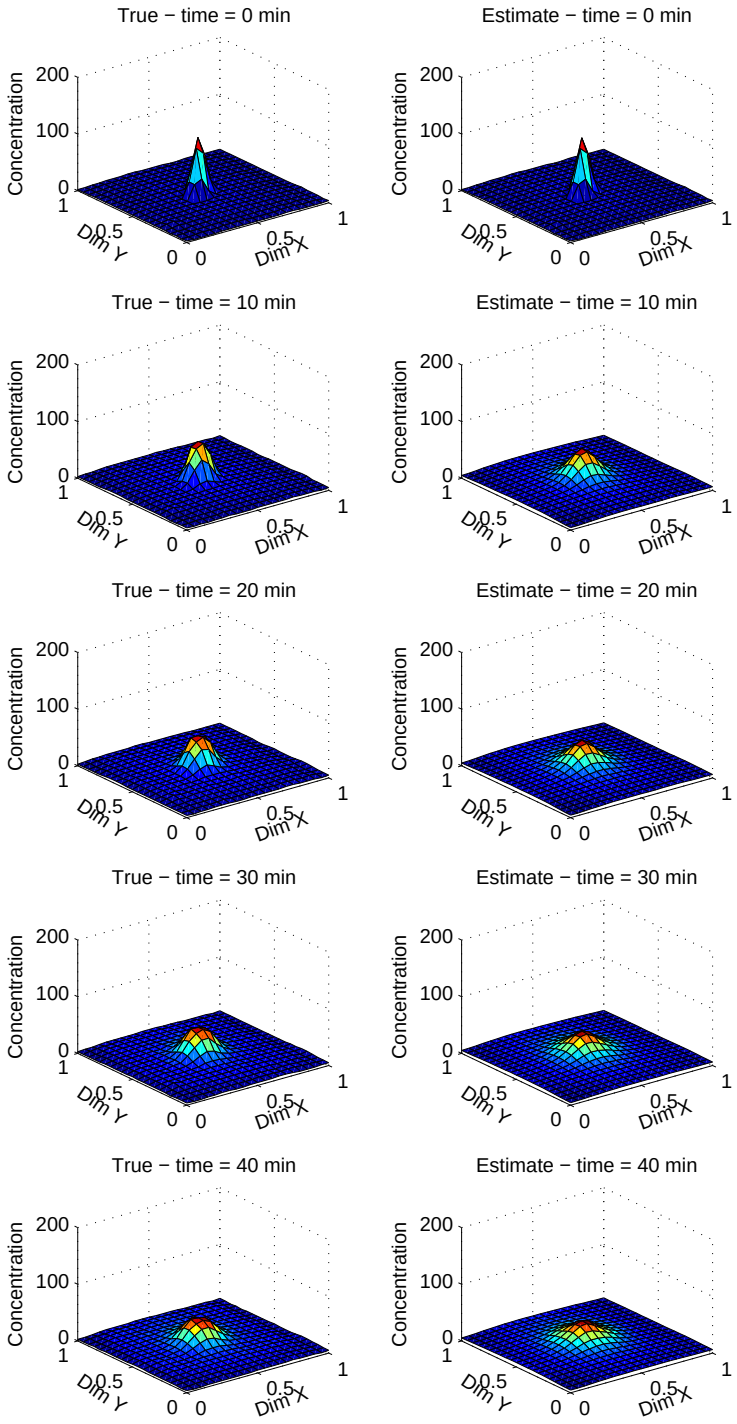

Figure 4.6: Complete measurements surface (left) and estimated surface(right).

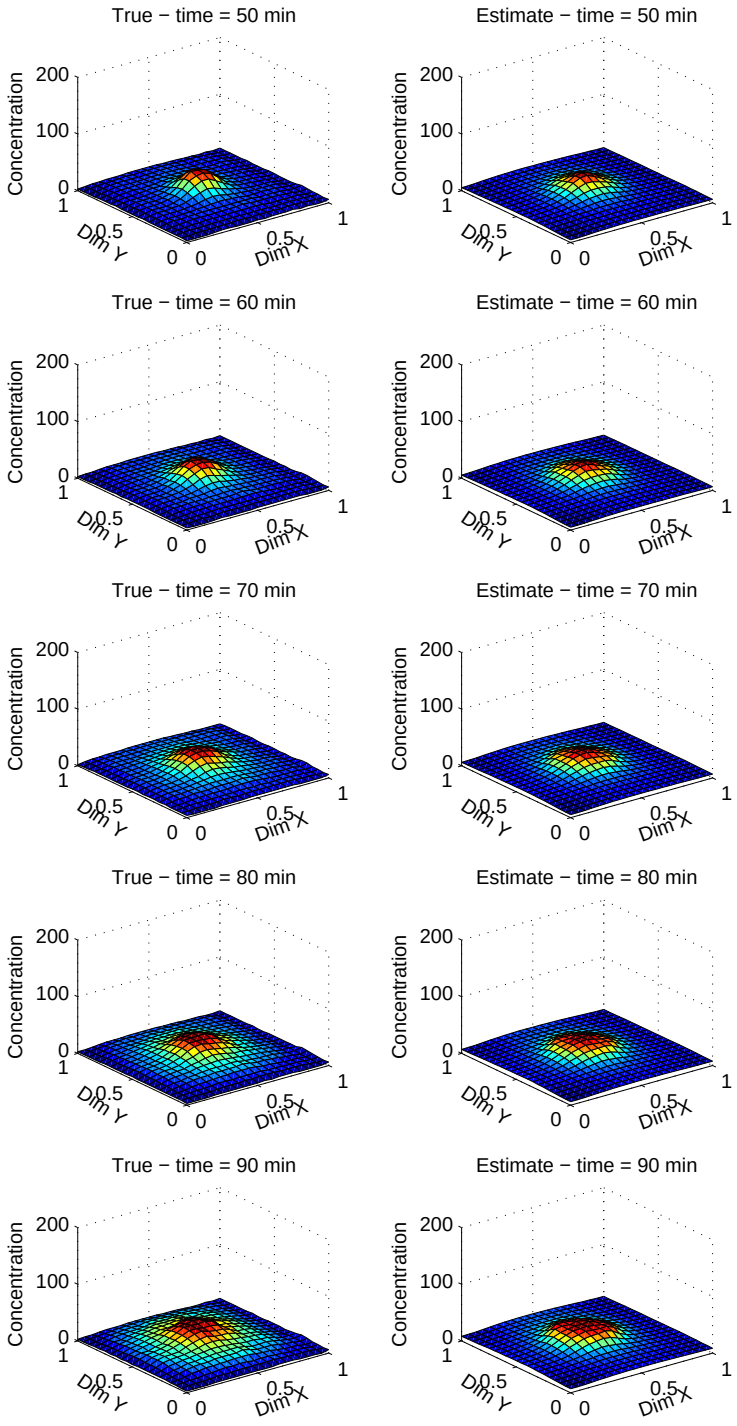

Figure 4.7: Complete measurements surface (left) and estimated surface(right).

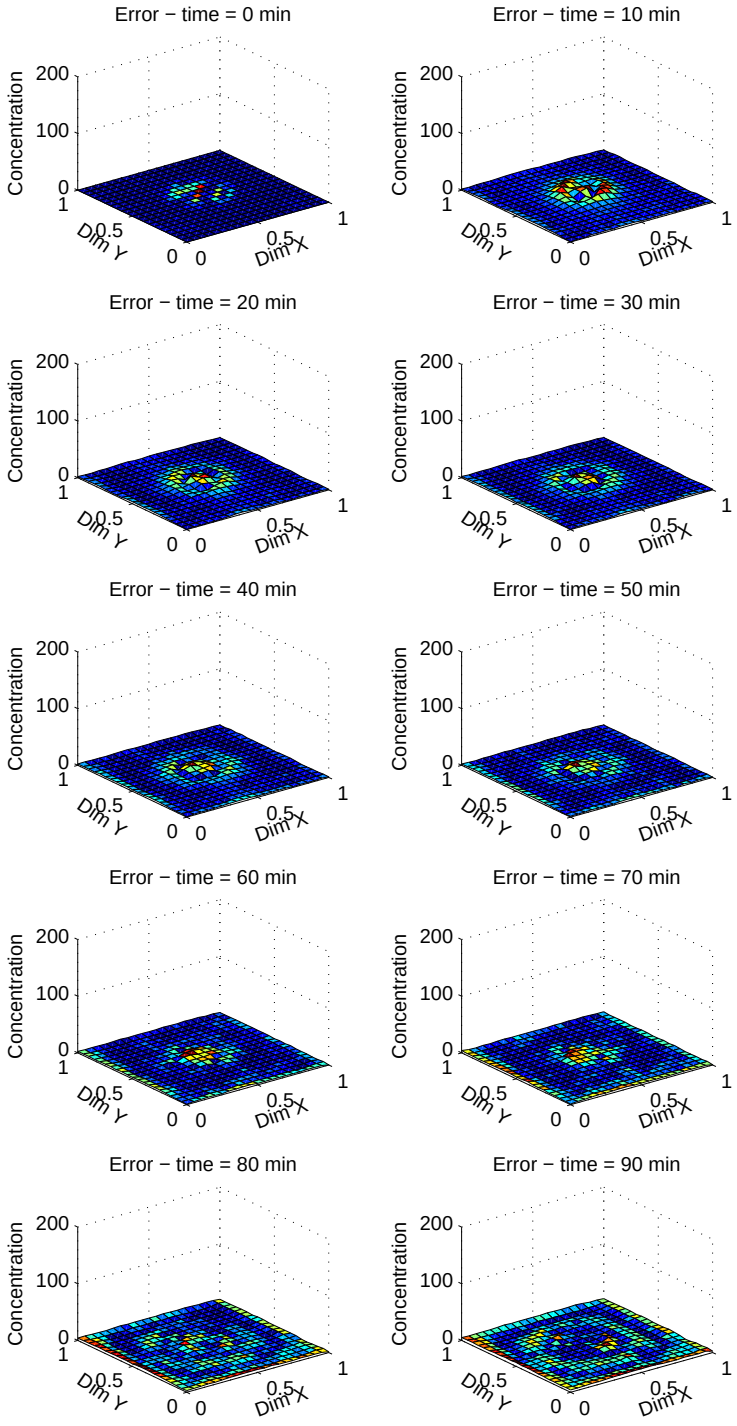

Figure 4.8: Absolute difference of error.

Chapter 5

Conclusions and Future Work

A test platform for state estimation of diffusion processes was developed and the efficacy of the state estimator was demonstrated. A common process in biological systems is the mass transport process of oxygen diffusion through tissues, known as Fick's first law. The action of dye diffusing in gelatin mimics the dynamics expressed by Fick's first law. The platform was used to test the diffusion of dye through gelatin with approximately 15% error even though the dynamic model was not well fit to the experiment data. The test platform can also serve to test biological sensors such as transition metal complexes or metal chelates which are mixed with plastics or injected into liposomes to form sensors and read using confocal microscopes. The test platform can also be used to verify estimation extensions of the state estimation technique described here.

The Karhunen-Loéve-Galerkin reduced-order model was shown to reproduce the dynamics of a PDE system with only three or four ODEs. The empirical Karhunen-Loéve basis was shown to have a clear advantage over a Fourier basis for reproducing known dynamics with known source terms. For systems where the source terms or actuators are not known the empirical basis will produce low fidelity results. Many of the *in silico* cancer models describe phenomena on multiple length scales. Using a wavelet-Galerkin method may be advantageous owing to the multi-resolution nature and may provide a more generalized set of candidate functions for the Galerkin projection.

The single biggest improvement which could be made to this system is development of rigorous sensor placement strategies and observability requirements. The placement and number of sensors in the numerical studies section were iterated until the estimator had low error. Characteristics about the system will be known such as the principal modes, composition of the sample and

properties of the spatial domain which should be incorporated into optimally placing sensors. Use of the state estimator in a biological system with optical contactless point sensors will require further devlopment. Contactless beads will require examination of a sample under high magnification making batch polling of the sensors difficult if not impossible. A method for optimally incorporating sensor measurements that are asynchronous or delayed will provide a necessary ability for use in a tissue test system.

Further out, application of this method to linear parabolic PDE description of tumor models could be used to guide design of biological experiments. Simulations and investigation of sensing requirements in a 2D tumor model as described in the section 1.1 or a more sophisticated 3D model and performing a change of basis to 2D could be performed. Designing a tissue sample with known properties such as cell phenotype distribution, nutrient sources, scaffolding material, etcetera could be modeled *in silico* and simulated. Using a tissue engineering tool such as a bioprinter a tissue sample could be constructed to experimentally verify the simulation results. The results of the simulations could be used to aid in designing biological experiments. Contactless optical biosensors such as liposomes or beads could be used to measure system properties, while deposition of nutrients and anticancer agents could serve as actuators. In order to actively control the system state the Karhunen-Loéve-Galerkin model will have to be implemented in a fashion to accept control inputs.

Use of the Karhunen-Loéve-Galerkin reduced-order model for state estimation in a biologically relevant medium has been demonstrated and further development will prove useful as biological modeling, simulation, and control continues to mature.

Bibliography

[1] G. Welch ad G. Bishop. An introduction to the kalman filter. Technical Report T.R. 95-041, 2006.

[2] B.B. Aldridge, J.M. Burke, and P.K. Sorger. Physiochemical modelling of cell signalling pathways. *Nature Cell Biology*, 8(11):1195–1203, 2006.

[3] K. Amarantuga, J.R. Williams, S. Qian, and J. Weiss. Wavelet-galerkin solutions for one-dimensional partial differential equations. *Int. J. Num. Mthds. Eng.*, 37:2703–2716, 1994.

[4] A.R.A Anderson. A hybrid mathematical model of solid tumour invasion: the importance of cell adhesion. *Mathematical Medicine and Biology*, 22:163–186, 2005.

[5] A.R.A Anderson, K.A. Rejniak, P. Gerlee, and V. Quaranta. Microenvironment driven invasion: a multiscale multimodel investigation. *Journal of Mathematical Biology*, 58:579–624, 2009.

[6] C.A. Andrews, J.M. Davies, and G.R. Schwartz. Adaptive data compression. *Proceedings of the IEEE*, 55(3):267–277, 1967.

[7] R.P. Araujo and D.L.S. McElwain. A history of the study of solid tumour growth: The contribution of mathematical modelling. *Bulletin of Mathematical Biology*, 66:1039–1091, 2004.

[8] A. Armaou and P.D. Christofides. Nonlinear feedback control of parabolic partial differential equation systems with time-dependent spatial domains. *Journal of Mathematical Analysis and Applications*, 239:124–157, 1999.

[9] A. Armaou and P.D. Christofides. Finite-dimensional control of nonlinear parabolic pde systems with time-dependent spatial domains using empirical eigenfunctions. *Int. J. Appl. Math. Comput. Sci.*, 11(2):287–317, 2001.

[10] A. Armaou and P.D. Christofides. Robust control of parabolic pde systems with time-dependent spatial domains. *Automatica*, 37:61–69, 2001.

[11] J. Baker, A. Armaou, and P.D. Christofides. Nonlinear control of incompressible fluid flow: Application to burgers' equation and 2d channel flow. *Journal of Mathematical Analysis and Applications*, 252:230–255, 2000.

[12] J. Baker and P.D. Christofides. Output feedback control of parabolic pde systems with nonlinear spatial differential operators. *Ind. Eng. Chem. Res.*, 38:4272–4380, 1999.

[13] J. Baker and P.G. Christofides. Finite-dimensional approximation and control of non-linear parabolic pde systems. *Int. J. Control*, 73(5):439–456, 2000.

[14] M.J. Balas. Feedback control of linear diffusion processes. *Int. J. Control*, 29(3):523–533, 1979.

[15] M.J. Balas. The galerkin method and feedback control of linear distributed parameter system. *Journal of Mathematical Analysis and Applications*, 91:523–533, 1983.

[16] R. Becker, M. Garwon, and R. King. Robust control of separated shear flows in simulation and experiment. *Proceedings of the European Control Conference*, 2003.

[17] G. Berkooz, P. Holmes, and J.L. Lumley. The proper orthogonal decomposition in the analysis of turbulent flows. *Annu. Rev. Fluid Mech.*, 25:539–575, 1993.

[18] G. Beylkin and J.M. Keiser. On the adaptive numerical solution of nonlinear partial differential equations in wavelet bases. *Journal of Computational Physics*, 132:233–259, 1997.

[19] S.M. Borisov and I. Klimant. Blue led excitable temperature sensors based on a new europium(iii) chelate. *Journal of Fluorescence*, 18:581–589, 2008.

[20] S.M. Borisov, T. Mayr, and I. Klimant. Poly(styrene-block-vinlypyrrolidone) beads as a versatile material for simple fabrication of opitcal nanosensors. *Analytical Chemistry*, 80:573–582, 2008.

[21] K. Boryczko, W. Dzwinel, and D.A. Yuen. Dynamical clustering of red blood cells in capillary vessels. *Journal of Molecular Modeling*, 9:16–33, 2003.

[22] A.C. Burton. Rate of growth of solid tumours as a problem of diffusion. *Growth*, 30:157–176, 1966.

[23] H.M. Byrne. Dissecting cancer through mathematics: from the cell to the animal model. *Nature Reviews Cancer*, 10:221–230, 2010.

[24] J.F. Carrier and G. Stephanopoulos. Wavelet-based modulation in control-relevent process identification. *AIChe Journal*, 44(2):341–360, 1998.

[25] F. Castilione and B. Piccoli. Optimal control in a model of dendritic dell transfection cancer immunotherapy. *Bulletin of Mathematical Biology*, 68:173–185, 2006.

[26] M.A.J. Chaplain, S.R. McDougall, and A.R.A. Anderson. Mathematical modeling of tumor-induced angiogenesis. *Annual Review of Biomedical Engineering*, 8:233–257, 2006.

[27] C. Chen and H. Chang. Accelerated disturbance damping of an unknown distributed system by nonlinear feedback. *AIChE Journal*, 38(9):1461–1476, 1992.

[28] T. Chiu and P.D. Christofides. Nonlinear control of particulate processes. *AIChE Journal*, 45(6):1279–1297, 1999.

[29] P.D. Christofides and P. Dauotidis. Finite-dimensional control of parabolic pde systems using approximate inertial manifolds. *Journal of Mathematical Analysis and Applications*, 216:398–420, 1997.

[30] L.G. de Pillis and A. Radunskaya. A mathematical tumor model with immune resistance and drug therapy: an optimal control approach. *Journal of Theoretical Medicine*, 3:79–100, 2001.

[31] D.P. Dee. Simplification of the kalman filter for meterological data assimilation. *Quarterly Journal of the Royal Meteorological Society*, 117:365–384, 1991.

[32] P. D'haeseleer, S. Liang, and R. Somogyi. Genetic network inference: from co-expression clustering to reverse engineering. *Bioinformatics*, 16(8):707–726, 2000.

[33] P. DuChateau and D. Zachmann. *Applied Partial Differential Equations*. Harpter & Row, Publishers, Inc., New York, 1989.

[34] P. Eiselt, B.-S. Kim, B. Chacko, B. Isenberg, M.C. Peters, K.G. Greene, W.D. Roland, A.B. Loebsack, K.J.L. Burg, C. Culberson, C.R. Halberstadt, W.D. Holder, and D.J. Mooney. Development of technologies aiding large-tissue engineering. *Biotechnology Progress*, 14:134–140, 1998.

[35] G. Evensen. Using the extended kalman filter with a multilayer quasi-geostrophic ocean model. *Journal of Geophysical Research*, 97(C11):17905–17924, 1992.

[36] R. Everson and L. Sirovich. Karhunen-loéve procedure for gappy data. *Journal of the Optical Society of America*, 12(8):1657–1664, 1995.

[37] B.F. Farrell and P.J. Ioannou. State estimation using a reduced-order kalman filter. *Journal of Atmospheric Sciences*, 58:3666–3680, 2001.

[38] K.R. Fister and J.C. Panetta. Optimal control applied to cell-cycle-specific cancer chemotherapy. *SIAM Journal on Applied Mathematics*, 60(3):1059–1072, 2000.

[39] C. Foias, M.S. Jolly, G.R. Sell, and E.S. Titi. On the computation of inertial manifolds. *Physics Letters A*, 131(7,8):433–436, 1988.

[40] J. Folkman. Tumor angiogenesis factor. *Cancer Research*, 34:2109–1974, 1974.

[41] J. Folkman, E. Merler, C. Abernathy, and G. Williams. Tumor behavior in isolated perfused organs: In vitro growth and metastases of biopsy material in rabbit thyroid and canine intestinal segment. *Annals of Surgery*, 164:491–502, 1966.

[42] J. Folkman, E. Merler, C. Abernathy, and G. Williams. Isolation of tumor factor responsible for angiogenesis. *Journal of Experimental Medecine*, 138:745–753, 1973.

[43] H.B. Frieboes, M.R. Edgerton, J.P. Fruehauf, F.R.A.J Rose, and L.K. Worrall. Prediction of drug response in breast cancer using integrative experimental/computational modeling. *Cancer Research*, 69:4484–4492, 2010.

[44] I. Fukumori and P. Malanotte-Rizzoli. An approximate kalman filter for ocean data assimilation; an example with an idealized gulf stream model. *Journal of Geophysical Research*, 100(C12):6777–6793, 1994.

[45] R. Ghanem and F. Romeo. A wavelet-based approach for model and parameter identification of non-linear systems. *International Journal of Non-Linear Mechanics*, 36(5):835–859, 2001.

[46] M.S. Gockenbach. *Partial Differential Equations: Analytical and Numerical Methods*. Society for Industrial and Applied Mathematics, Philadelphis, USA, 2002.

[47] D. Gottlieb and S.A. Orszag. *Numerical Analysis of Spectral Methods: Theory and Applications*. Society for Industrial and Applied Mathematics, Montpelier, Vt, 1977.

[48] M.D. Graham and I.G. Kevrekidis. Alternative approaches to the karhunen-loéve decomposition for model reduction and data analysis. *Computers & Chemical Engineering*, 20(5):495–506, 1996.

[49] H.S.N. Greene. Heterlogous transplantation of mammalian tumors. *Journal of Experimental Medicine*, 73:461–473, 1961.

[50] H.P. Greenspan. Models for the growth of a solid tumor by diffusion. *Studies in Applied Mathematics*, 52:317–340, 1972.

[51] M.S. Grewal and A.P. Andrews. *Kalman Filtering: Theory and Practice*. Wiley-Interscience, New York, second edition, 2001.

[52] D.V. Griffiths and I.M. Smith. *Numerical Methods for Engineers*. Hartnoll Ltd, Bodmin, Great Britain, 1991.

[53] J. Gunther, R. Beard, J. Wilson, T. Oliphant, and W. Stirling. Fast nonlinear filtering via galerkin's method. 36:101–127, 2002.

[54] P. Hahnfeldt and D. Panigraphy. Tumor development under angiogenic signaling: A dynamical theory of tumor growth, treatment response, and postvascular dormancy. *Cancer Research*, 59:4770–4775, 1999.

[55] I. Hemmila and V. Laitala. Progress in lanthanides as luminescent probes. *Journal of Fluorescence*, 15(4):529–542, 2005.

[56] A.V. Hill. The diffusion of oxygen and lactic acid through tissues. *Proceedings of the Royal Society of London. Series B, Containing Papers of a Biological Character*, 104(728):39–96, 1928.

[57] P. Holmes, J.L. Lumley, and G. Berkooz. *Turbulence, Coherent Structures, Dynamical Systems and Symmetry*. Cambridge University, Cambridge, UK, 1996.

[58] I. Hoteit, D.-T. Pham, and J. Blum. A simplified reduced order kalman filtering and application to altimetric data assimilation in tropical pacific. *Journal of Marine Systems*, 36:101–127, 2002.

[59] H. Hotelling. Analysis of a complex of statistical variables into principal components. *J. Educational Psychol.*, 1933.

[60] S.Y. Im, G.E. Khalil, J. Callis, B.H. Ahn, M. Gouterman, and Y. Xia. Synthesis of polystyrene beads loaded with dual lumiphors for self-referenced oxygen sensing. *Talanta*, 67:492–497, 2005.

[61] E. Kalnay. *Atmospheric Modeling, Data Assimilation and Predictability*. Cambridge University Press, Cambridge, UK, 2003.

[62] E. Kalnay, H. Li, T. Miyoshi, S.C. Yang, and J. Ballabrera-Poy. 4-d-var or ensemble kalman filter. *Tellus*, 59A:758–773, 2007.

[63] K. Karhunen. Zur spektraltheorie stochastischer prozesse. *Ann. Acad. Sci. Fennicae*, Ser A1(34):1941–1956, 1946.

[64] H.R. Karimi and B. Lohman. Haar wavelet-based robust optimal control for vibration reduction of vehicle engine-body system. *Electrical Engineering (Archiv fur Elektrotechnik)*, 89(6):469–478, 2007.

[65] K. Kellner, G. Liebsch, I. Klimant, O.S. Wolfbeis, T. Blunk, M.B. Schulz, and A. Göpferich. Determination of oxygen gradients in engineered tissue using a flourescent sensor. *Biotechnology and Bioengineering*, 80(1):73–83, 2002.

[66] S. Khalil, F. Nam, and W. Sun. Multi-nozzle deposition for construction of 3d biopolymer tissue scaffolds. *Rapid Prototyping Journal*, 11(1):9–17, 2005.

[67] T. Kijewski and A. Kareem. Wavelet transforms for system identification in civil engineering. *Computer-Aided Civil and Infrastructure Engineering*, 18:339–355, 2003.

[68] M. Kirby and L. Sirovich. Application of the karhunen-loéve procedure for the characterization of human faces. *IEEE Transactions on Pattern Analysis and Machine Intelligence*, 12(1):103–108, 1990.

[69] D. Kirschner, S. Lenhart, and S. Serbin. Optimal control of the chemotherapy of hiv. *Journal of Mathematical Biology*, 35:775–792, 1997.

[70] I. Klimant and O.S. Wolfbeis. Oxygen-sensitive luminescent materials based on silicone-soluble ruthenium diimine complexes. *Analytical Chemistry*, 67:3160–3166, 1995.

[71] W. Kolch. Defining systems biology: through the eyes of a biochemist. *IET Syst Biol*, 2(1):5–7, 2008.

[72] D.D. Kosambi. Statistics in function space. *Journal of Indian Mathematical Society*, 7:76–88, 1943.

[73] A.K. Laird. Dynamics of tumor growth: comparison of growth rates and extrapolation of growth curve to one cell. *British Journal of Cancer*, 18:490–502, 1965.

[74] S. Lall, J.E. Marsden, and S. Glavinski. A subspace approach to balanced truncation for model reduction of nonlinear control systems. *International Journal on Robust and Nonlinear Control*, 12(6):519–535, 2002.

[75] J.L. Lankelma, H. Dekker, R.F. Luque, S. Luykx, K. Hoekman, P.J. van Diest, and H.M. Pinedo. Doxorubicin gradients in human breast cancer. *Clinical Cancer Research*, 5:1703–1707, 1999.

[76] U. Ledzewicz and H. Schättler. Optimal bang-bang controls for a two-compartment model in cancer chemotherapy. *Journal of Optimization Theory and Applications*, 114(3):609–637, 2002.

[77] U. Ledzewicz and H. Schättler. Optimal and suboptimal protocols for a class of mathematical models of tumor anti-angiogenesis. *Journal of Theoretical Biology*, 252:295–312, 2008.

[78] R.J. LeVeque. *Finite Difference Methods for Ordinary and Partial Differential Equations.* Society for Industrial and Applied Mathematics, Philadelphia, USA, 2007.

[79] H.W. Liepmann. Aspects of the turbulence problem. part ii. *Agnew. Math. Phys.*, 3:407–426, 1952.

[80] M. Loéve. Fonctions alétores de second ordre. *Comptes Rendus de lÁcadémie de Sciences, Série I: Mathématique*, 220:469, 1945.

[81] J.L. Lumley and R.E. Meyer. Coherent structures in turbulence. *Transition and Turbulence*, 1981.

[82] N. Mantzaris, S. Webb, and H.G. Othmer. Mathematical modeling of tumor-induced angiogenesis. *Journal of Mathematical Biology*, 49:111–187, 2004.

[83] M. Marion and R. Temam. Nonlinear galerkin methods. *SIAM Journal of Numerical Analysis*, 26(5):1139–1157, 1989.

[84] D. Maroudas. Multiscale modeling of hart materials: Challenges and opportunities for chemical engineering. *AIChE Journal*, 46(5):878–882, 2000.

[85] P.S. Maybeck. *Stochastic models, estimation and control*, volume 1. Academic Press, Inc., New York, NY, 1979.

[86] K.P. McNamara and Z. Rosenzweig. Dye-encasulating liposomes as fluorescence-based oxygen nanosensors. *Analytical Chemistry*, 70:4853–4859, 1998.

[87] B.C. Moore. Principal component analysis in linear systems: Controllability, observability, and model reduction. *IEEE Transactions on Automatic Control*, AC-26(1):17–32, 1981.

[88] S. Nagl and O.S. Wolfbeis. Optical multiple chemical sensing: status and current challenges. *Analyst*, 132:507–511, 2007.

[89] M. Nakamura. Ink jet three-dimensional digital fabrication for biological tissue manufacturing: Analysis of alginate microgel beads produced by ink jet droplets for three dimensional fabrication. *Journal of Imaging Science and Technology*, 56(6):060201–060201–6, 2008.

[90] N. Nath, T. Burg, D.M. Dawson, and E. Iyasere. Optimizaing antiangiogenic therapy for tumor minimization. Technical Report CU/CRB/09/14/09/2, 2009.

[91] A. Neagu, K. Jakab, R. Jamison, and G. Forgacs. Role of physical mechanisms in biological self-organization. *Physical Review Letters*, 95(17):178104(4), 2005.

[92] A.J. Newman. Model reduction via the karhunen-loéve expansion part i: An exposition. Technical Report T.R. 96-32, 1996.

[93] A.J. Newman. Model reduction via the karhunen-loéve expansion part ii: Some elementary examples. Technical Report T.R. 96-33, 1996.

[94] B.R. Noack, P. Papas, and P.A. Monkewitz. The need for a pressure-term representation in empirical galerkin models of incompressible shear flows. *Journal of Fluid Mechanics*, 523:339–365, 2005.

[95] B. Novak and J.J. Tyson. Design principles of biochemical oscillators. *Nature Reviews Molecular Cell Biology*, 9:981–991, 2008.

[96] A.M. Obukhov. Statistical description of continuous fields. *Trudy Geophys. int. Aked. Nauk. SSSR*, 24:3–42, 1954.

[97] E.L. Ortiz. The tau method. *Society for Industrial and Applied Mathematics*, 6(3):480–492, 1969.

[98] E.E. Osgood. A unifying concept of the etiology of the leukemias, lymphomas, and cancers. *Journal of the National Cancer Institute*, 18:155–166, 1957.

[99] D.B. Papkovsky, T. O'Riordan, and A. Soini. Phosphorescent porphyrin probes in biosensors and senstive bioassays. *Biochemical Society Transactions*, 28(2):74–77, 2000.

[100] D.B. Papkovsky, G.V. Ponomarev, W.T Trettnak, and P. O'Leary. Phosphorescent complexes of porphyrin ketones: Optical properties and application to oxygen sensing. *Analytical Chemistry*, 67:4112–4117, 1995.

[101] H.M. Park and D.H. Cho. The use of the karhunen-loéve decomposition for the modeling of distributed parameter systems. *Chemical Engineering Science*, 51(1):81–98, 1996.

[102] K. Pearson. On lines and planes of closest fit to systems of points in space. *Phil. Mag.*, 6th series, 1901.

[103] M.E. Pepper, C.A. Parzel, T. Burg, T. Boland, K.J.L. Burg, and R.E. Groff. Design and implementation of a two-dimensional inkjet bioprinter. *Conf Proc IEEE Eng Med Biol Soc 2009*, pages 6001–6005, 2009.

[104] D.T. Phame, J. Verron, and M.C. Roubaud. A singular evolutive extended kalman filter for data assimilation in oceanography. *Journal of Marine Systems*, 16:323–340, 1998.

[105] A.J. Pirmeau, A. Rendon, D. Hedley, L. Lilge, and I.F. Tannock. The distribution of anti-cancer drug doxorubicin in relation to blood vessels in solid tumors. *Clinical Cancer Research*, 11(24):8782–8788, 2005.

[106] V.S. Pougachev. General theory of the correlations of random functions. *Izv. Akad. Nauk. SSSR. Math. Ser.*, 285:401–402, 1953.

[107] S. Qian and J. Weiss. Wavelets and the numerical solution of partial differential equations. *Journal of Computational Physics*, 106:155–175, 1993.

[108] V. Quaranta, K.A. Rejniak, P. Gerlee, and A.R.A. Anderson. Invasion emerges from cancer cell adaptation to competitive microenvironments: Quantitative prediction from multiscale mathematical models. *Seminars in Cancer Biology*, 18:338–348, 2008.

[109] A. Quarteroni, M. Tuveri, and A. Veneziani. Computational vascular fluid dynamics: problems, models and methods. *PNAS*, 97(9):4649–4653, 2000.

[110] J.D. Rambo. *Reduced-Order Modeling of Multiscale Turbulent Convection: Application to Data Center Thermal Management*. PhD thesis, Georgia Institute of Technology, May 2006.

[111] C.V. Rao, D.M. Wolf, and A.P. Arkin. Control, exploitation and tolerance of intracellular noise. *Nature*, 420:231–237, 2002.

[112] C.W. Rowle. Model reduction for fluids, using balanced proper orthogonal decomposition. *International Journal on Bifurcation and Chaos*, 15(3):997–1013, 2005.

[113] C.W. Rowley, I.G. Kevrekidis, J.E. Marsden, and K. Lust. Reduction and reconstruction for self-similar dynamical systems. *Nonlinearity*, 16:1257–1275, 2003.

[114] C.W. Rowley and J.E. Mardsen. Reconstruction equations and the karhunen-loéve expansion for systems with symmetry. *Physica D - Nonlinear Phenomena*, 142:1–19, 2000.

[115] K. Sayood. *Introduction to Data Compression*. Academic Press, 2000.

[116] W.E Schiesser and G.W. Griffiths. *A Compendium of Partial Differential Equation Models*. Cambridge University Press, Cambridge, UK, 2009.

[117] S.Y. Shvartsman and I.G. Kevrekidis. Nonlinear model reduction for control of distributed systems: a computer-assisted study. *AIChE Journal*, 44(7):1579–1595, 1998.

[118] R.M. Shymko and M.A.J. Chaplain. Cellular and geometric control of tissue growth and mitotic instability. *Journal of Theoretical Biology*, 63:355–374, 1976.

[119] J. Sinek, H. Sanga, and X. Zheng H.B.

[120] E.D. Sontag. Molecular systems biology and control. *European Journal of Control*, 11:396–435, 2005.

[121] J. Stewart. *Calculus*. Brooks/Cole-Thomson Learning, Belmont, CA, fifth edition, 2003.

[122] A. Tangborn and S.Q. Zhang. Wavelet transform adapted to an approximate kalman filter system. *Applied Numerical Mathematics*, 33:307–316, 2000.

[123] R.H. Thomlinson and L.H. Gray. The histological structure of some human lung cancers and the possible implications for radiotherapy. *British Journal of Cancer*, 9:539–549, 1955.

[124] E.S. Titi. On approximate inertial manifolds to the navier-stokes equations. *Journal of Mathematical Analysis and Applications*, 149:540–557, 1990.

[125] A.A. Townsend. *The Structure of Turbulent Shear Flow*. Cambridge University Press, Cambridge, UK, 1956.

[126] M. Turk and A. Pentland. Eigenfaces for recognition. *Journal of Cognitive Neuroscience*, 3(1):71–86, 1991.

[127] J.J. Tyson, K.C. Chen, and B. Novak. Sniffers, buzzers, toggles and blinkers: dynamics of regulatory and signaling pathways in the cell. *Current Opinion in Cell Biology*, 15:221–231, 2003.

[128] K. Willcox and J. Peraire. Balanced model reduction via the proper orthogonal decomposition. *AAIA Journal*, 40(11):2323–2330, 2002.

[129] T.M. Yi, Y. Huang, M.I. Simson, and J. Doyle. Robust pefect adaptation in bacterial chemotaxis through integral feedback control. *PNAS*, 97(9):4649–4653, 2000.